Helsinki University of Technology
Department of Electrical and Communications Engineering
Optoelectronics Laboratory
Espoo, Finland 2003

Fabrication and characterization of GaInNAs quantum structures

Teppo Hakkarainen

Dissertation for the degree of Doctor of Science in Technology to be presented with due permission of the Department of Electrical and Communications Engineering for public examination and debate in Auditorium S1 at Helsinki University of Technology (Espoo, Finland) on the 13th of June, 2003, at 12 o'clock noon.

Helsinki University of Technology
Department of Electrical and Communications Engineering
Optoelectronics Laboratory
P. O. Box 3500
FIN-02015 HUT
Finland
Tel: +358 9 451 3121
Fax: +358 9 451 3128

ISBN 951-22-6516-8 (printed version)
ISBN 951-22-6517-6 (electronic version)

Picaset Oy
Helsinki 2003

ABSTRACT

The fabrication and the structural and optical properties of bulk, quantum well, and quantum dot structures prepared of GaAsN and GaInNAs III-V compound semiconductors are studied in this thesis. Metalorganic vapor phase epitaxy is used to grow epitaxial layers on GaAs. The composition of the grown structures is investigated by x-ray diffraction. The nitrogen concentration of the GaAsN and GaInNAs layers is found to be strongly dependent on the growth temperature and the molar flow ratios of the different precursors. It is shown that an increase in the indium concentration of GaInNAs results in a decrease of the nitrogen incorporation.

Photoluminescence spectroscopy is employed to study the optical properties of the fabricated epitaxial structures. The optical quality of quantum well structures is found to decrease with increasing nitrogen concentration. However, in-situ and post-growth thermal annealing procedures as well as post-growth laser treatment are investigated and used to improve the optical properties. Luminescence wavelengths of up to 1.55 μm are observed from GaInNAs quantum well structures.

The effect of nitrogen on the optical properties of various self-assembled quantum dot structures is studied. The surface morphology of these structures is investigated by atomic force microscopy. Although the incorporation of nitrogen into GaIn(N)As quantum dots is found to be negligible, the size and the areal density of the self-organized GaIn(N)As islands can be controlled and the optical properties improved by varying the nitrogen precursor flow. It is found that the luminescence wavelength and intensity of GaInAs quantum dots in the 1.3 μm wavelength range can be increased by embedding the islands in a GaInNAs barrier layer. Also strain-induced GaInNAs quantum dots are fabricated using InP islands as stressors.

PREFACE

The work for this thesis has been carried out at Optoelectronics Laboratory of Helsinki University of Technology during 2000-2002. I want to express my gratitude to Professor Turkka Tuomi for an opportunity to work in the field of semiconductor epitaxy and to Professor Harri Lipsanen, the supervisor of this thesis, for the support and guidance during this time.

I am most of all greatly indebted to Dr. Markku Sopanen for his continuous instructions during this work. I want to especially thank Juha Toivonen for his many advice and fruitful collaboration in the epitaxial growth. I am grateful to all the personnel of the laboratory. National Graduate School in Material Physics is acknowledged for the financial support of this work.

Finally, I want to thank my mother Ulla and my sister Taija for their endless support, interest and encouragement during this work.

Espoo, February 2003 Teppo Hakkarainen

LIST OF PUBLICATIONS

This thesis consists of an overview and the following publications:

I J. Toivonen, T. Hakkarainen, M. Sopanen, and H. Lipsanen, *High nitrogen composition GaAsN by atmospheric pressure metalorganic vapor-phase epitaxy*, Journal of Crystal Growth **221**, 456-460 (2000).

II T. Hakkarainen, J. Toivonen, M. Sopanen, and H. Lipsanen, *Self-assembled GaIn(N)As quantum dots: Enhanced luminescence at 1.3 μm*, Applied Physics Letters **79**, 3932-3934 (2001).

III T. Hakkarainen, J. Toivonen, M. Sopanen, and H. Lipsanen, *GaInNAs quantum well structures for 1.55 μm emission on GaAs by atmospheric pressure metalorganic vapor phase epitaxy*, Journal of Crystal Growth **234**, 631-636 (2002).

IV J. Toivonen, T. Hakkarainen, M. Sopanen, H. Lipsanen, J. Oila, and K. Saarinen, *Observation of defect complexes containing Ga vacancies in GaAsN*, Applied Physics Letters **82**, 40-42 (2003).

V T. Hakkarainen, J. Toivonen, M. Sopanen, and H. Lipsanen, *Wavelength extension of GaInAs/GaIn(N)As quantum dot structures grown on GaAs*, Journal of Crystal Growth **248**, 339-342 (2003).

VI J. Toivonen, T. Tuomi, J. Riikonen, L. Knuuttila, T. Hakkarainen, M. Sopanen, H. Lipsanen, P. J. McNally, W. Chen, and D. Lowney, *Misfit dislocations in GaAsN - GaAs interface*, accepted to Journal of Materials Science: Materials in Electronics.

VII H. Koskenvaara, T. Hakkarainen, M. Sopanen, and H. Lipsanen, *Photoluminescence study of strain-induced GaInNAs/GaAs quantum dots*, Journal of Materials Science: Materials in Electronics **14**, 357-360 (2003).

VIII J. Toivonen, T. Hakkarainen, M. Sopanen, and H. Lipsanen, *Effect of post-growth laser treatment on optical properties of Ga(In)NAs quantum wells*, IEE proceedings – Optoelectronics **150**, 68-71 (2003).

AUTHOR'S CONTRIBUTION

The growth parameters and sample structures for all publications were planned by the author and the co-authors. The samples for publications II, III, V, and VII were grown by the author. For publications I and VIII the samples were grown by J. Toivonen and the author.

The photoluminescence studies for publications II, III, and V were carried out by the author. The photoluminescence studies for publication VIII were performed by J. Toivonen and the author.

The atomic force microscopy for publications II and V and the x-ray diffraction measurements for publication III were carried out by the author.

The author has written the manuscript for publications II, III, and V and has contributed to the data analysis and manuscripts for publications I, IV, and VI–VIII. The author has especially focused on the growth and study of long-wavelength GaInNAs quantum wells and GaInNAs quantum dot structures.

CONTENTS

1 INTRODUCTION

Semiconductor lasers operating at 1.3 and 1.55 μm wavelength are very important light sources in optical communications since the quartz fiber used as a transport media of light has dispersion and attenuation minima, respectively, at these wavelengths. These long-wavelength lasers have been traditionally fabricated on InP substrates using InGaAsP bulk layers and quantum wells (QWs) as an active material. However, this material system has relatively poor high-temperature characteristics and the power output is limited due to the poor electron confinement in the QWs. Therefore, there has been considerable effort for many years to fabricate long-wavelength laser structures on other substrates, especially on GaAs. The manufacturing costs of GaAs-based components are lower and the processing techniques are well developed.

GaAs is already successfully used in 850 nm vertical cavity surface-emitting lasers (VCSELs) which have become common in short-range optical communications. The incredible growth of the internet and data transmission has pushed the bit-rate requirements for local area and metro area networks from 100 Mbps to 10 Gbps. Therefore, there is a great demand for low-cost, 1.3 or 1.55 μm VCSELs that will operate uncooled under ambient conditions. While InGaAsP/InP material system is good for conventional edge-emitting lasers, it is difficult to realize the distributed Bragg reflector VCSEL mirrors with these materials.

One approach to achieve 1.3 μm emission on GaAs is to use self-assembled In(Ga)As quantum dots (QDs) in the active region. The QDs are three-dimensional self-organized In(Ga)As islands formed on GaAs when a critical thickness for island formation is exceeded. Although QD lasers have been predicted to have better characteristics than QW lasers, such as lower threshold current density and negligible temperature dependency, the commercial breakthrough has not yet occurred. Another approach was introduced in 1996 by Kondow *et al.* [1] who proposed a novel quaternary material GaInNAs, which could be grown lattice matched on GaAs and used to fabricate long-wavelength lasers with better temperature characteristics compared to InP-based lasers. The large bandgap bowing with nitrogen incorporation, observed first for the ternary alloy GaAsN by Weyers *et al.* [2] back in 1992, makes this material suitable for long-wavelength operation on GaAs. The study of these and other III-V-N alloys has been increasing ever since. The development of a GaInNAs/GaAs VCSEL operating at 1.3 μm wavelength has been rapid, and the first commercial products are about to arise. GaInNAs can also be used to improve the characteristics of multijunction solar cells and heterojunction bipolar transistors.

In this work, Ga(In)NAs bulk, QW and QD structures were grown by metalorganic vapor phase epitaxy. The optical properties of the structures were investigated by photoluminescence spectroscopy. Various methods were used to study

the structural properties of the samples. In publication I the growth conditions of GaAsN were optimized for high nitrogen composition of up to 5.6 %. In publication III GaInNAs QW structures were grown for 1.55 μm emission on GaAs. Defect complexes containing gallium vacancies and misfit dislocations in the GaAsN-GaAs interface were observed in publications IV and VI, respectively. The effect of post-growth laser treatment on Ga(In)NAs QWs was studied in publication VIII. In publication II self-assembled GaInNAs QDs were grown and an enhancement of 1.3 μm luminescence was observed. The use of GaInNAs as a barrier material for GaInAs QDs was investigated in publication V. Photoluminescence of strain-induced GaInNAs/GaAs QDs was studied in publication VII.

The structure of this overview is following. Chapter 2 introduces the main properties of the Ga(In)NAs alloys. The large bandgap bowing and electron effective mass as well as the major theoretical models used to explain the band structure are discussed. The device applications of GaInNAs are also briefly introduced. Chapter 3 describes the experimental methods, *i.e.*, metalorganic vapor phase epitaxy, photoluminescence spectroscopy, x-ray diffraction, and atomic force microscopy, employed by the author in this thesis. Chapters 4 and 5 summarize the results reported in publications I-VIII. Chapter 4 discusses the fabrication and properties of the bulk and QW structures and chapter 5 presents the fabrication and optical properties of the GaInNAs QD structures. The main results of this thesis are summarized in chapter 6.

2 Ga(In)NAs ALLOYS AND THEIR APPLICATIONS

This chapter introduces the main properties of the Ga(In)NAs alloys. Section 2.1 describes the effects of the nitrogen incorporation into GaAs. The huge bandgap bowing with increasing nitrogen incorporation is especially reviewed. Two most important theoretical models used to explain the GaInNAs bandstructure, *i.e.*, band anticrossing model and pseudopotential theory, are discussed in section 2.2. The band alignment in GaAsN and GaInNAs quantum structures is outlined in section 2.3. The device applications are briefly reviewed in section 2.4.

2.1 Effects of nitrogen in Ga(In)NAs

Due to the potential applications of GaInNAs in laser devices for optical communications considerable effort has been made in growing and studying this alloy system in the recent years. GaInNAs exhibits interesting new properties and differs considerably from the conventional III-V alloys, such as AlGaAs, GaInAs and GaInAsP, which are commonly employed in III-V device structures. Significant changes occur in the band structure compared to GaAs with incorporation of only a small percentage of nitrogen. These include a large redshift of the bandgap [2-8, publications I and III], an increase in the electron effective mass [9-11], a highly nonlinear pressure dependence of the bandgap [12, 13], a N-induced formation of new bands [7, 8, 13, 14], and a strong line width broadening of all transitions [7, 8, 14-16].

The key to understand the unusual properties of the Ga(In)NAs alloys is the large difference in size and electronegativity of arsenic and nitrogen atoms. The covalent radius and electronegativity of nitrogen are 0.068 Å and 3.04, respectively, compared to those of 0.121 Å and 2.18 for arsenic. A large difference in the atomic size causes deformation of the crystal lattice and the larger electronegativity of nitrogen favors electron localization around the nitrogen atom. In 1984 nitrogen was found to act as an isoelectronic impurity in GaAs, and the localized energy state formed by a single nitrogen atom was observed at 150-180 meV above the bottom of the conduction band [17]. In 1990 Liu *et al.* [18] reported about excitonic luminescence originating from nitrogen pair and cluster states located below the conduction band minimum of GaAs. The N concentration in their study was about 10^{17} cm^{-3}, *i.e.*, 0.001 %. More recently is has been found that the nitrogen incorporation leads to the strong redshift of the bandgap when the N concentration is increased to above 0.01 % [3]. However, the luminescence spectrum of GaAsN is still dominated by sharp excitonic transitions. The transformation from nitrogen acting as an isoelectronic impurity to a $GaAs_{1-x}N_x$ alloy

takes place at $x \approx 0.2$ %, and the excitonic transitions disappear from the luminescence spectrum [8].

The fundamental bandgap, E_g, of the conventional ternary III-V alloys is well represented by [19]:

$$E_g^{AB_{1-x}C_x} = xE_g^{AC} + (1-x)E_g^{AB} - bx(1-x). \quad (1)$$

The bowing parameter b is usually a constant with a value of less than 2 eV. In contrast, alloying GaAs with nitrogen leads to a giant bandgap bowing with increasing nitrogen molar fraction. Bandgap reductions of as large as 180 meV have been observed in $GaAs_{1-x}N_x$ with only 1 % of nitrogen [2-6]. Similar effects have been observed in InAsN [20], GaPN [21-22], InPN [23], GaAsSbN [24], and InSbN [25] alloys. Figure 1 shows the lattice constants and bandgaps of some III-V semiconductors. The lattice constant of GaAsN behaves linearly and decreases with increasing N content, since the lattice constant of cubic GaN is 4.5 Å. If linear approximation would apply, an increase of the bandgap energy from 1.42 eV of GaAs towards 3.2 eV of cubic GaN could be expected. Instead, the bandgap shows huge bowing with increasing N content. The N-induced decrease of the lattice constant can be compensated and the bandgap further reduced by adding indium to GaAsN. Therefore, it is possible to grow $Ga_{1-y}In_yN_xAs_{1-x}$ quaternary alloy that is lattice-matched to GaAs when $y \approx 3x$ and has a bandgap suitable for long-wavelength optical communications.

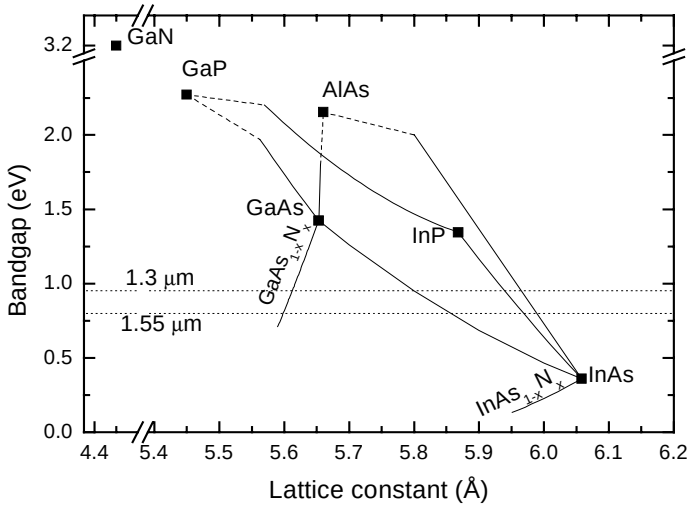

Figure 1. Bandgaps and lattice constants of some binary III-V semiconductors (squares). The continuous and dashed lines indicate direct and indirect bandgaps of ternary compounds, respectively. Areas between lines represent quaternary compounds. The fiber-optical communication wavelengths of 1.3 and 1.55 μm are also shown. GaInNAs can reach these wavelengths lattice matched to GaAs.

The bandgap of GaAsN has been investigated by photoluminescence [26, publication I], optical transmission [4, 5], spectroscopic ellipsometry [27], and electro- and photoreflectance [13, 28]. In publication I an attempt was made to quantify the composition dependence of E_g using equation 1 and a bowing parameter, b = 26 eV for x < 1 % and 16 eV for $x \geq 1$ %, as shown in figure 2. However, the calculated bandgap energies deviate considerably from the measured data especially for the higher values of x. One reason for this is that the photon energy of the photoluminescence peak is actually lower than the bandgap energy. Another reason is that the huge bandgap bowing of GaAsN is composition dependent [5, 29]. Other attempts have used an arbitrary quadratic function [27], a $x^{2/3}$ scaling rule [28] or a two level anticrossing model [13]. Tisch *et al.* [30] have recently proposed an empirical double exponential composition dependence of the bowing parameter. According to their model, the bowing parameter reaches 40 eV for dilute compositions, $x \approx 0.1$ %, and decreases strongly with increasing nitrogen molar fraction reaching a constant value of 7.5 eV for $x > 8$ %, beyond the present experimental range.

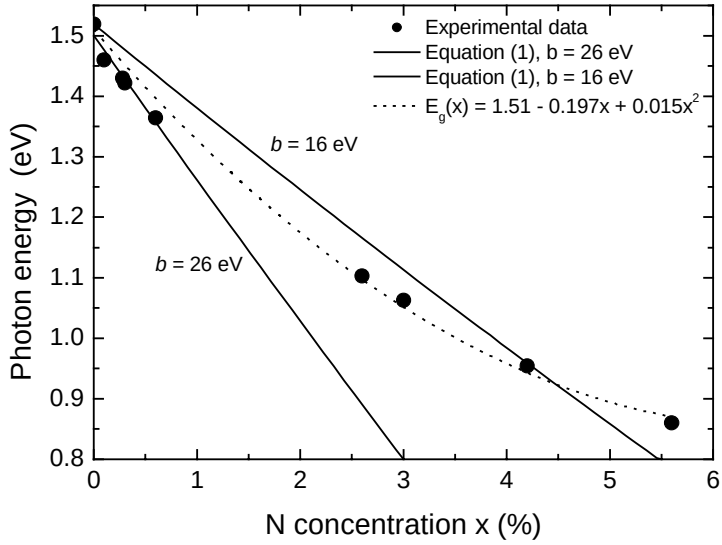

Figure 2. Photoluminescence peak energies for $GaAs_{1-x}N_x$ ($0 \leq x \leq 5.6$ %) samples measured at the temperature of 9 K. The solid lines are the bandgap energies fitted to data with a bowing parameter b of 16 and 26 eV for the average and the low N composition, respectively. For comparison, the dotted line shows a fit with a quadratic function.

The experimental studies of the electron effective mass reported so far give scattered and even contradictory results. Zhang *et al.*[31] reported a value of as high as 0.5 m_0 for 1 % of nitrogen in GaAsN/GaAs QWs and found that the effective mass decreased when the nitrogen incorporation was further increased. On the contrary,

Skierbiszewski *et al.*[9] reported a gradual increase of the effective mass at the bottom of the conduction band from 0.065 m_0 for GaAs to 0.12 m_0 for $GaAs_{0.97}N_{0.03}$. The gradual increase of the effective mass is supported by optically detected cyclotron resonance experiments [10], which indicate values of 0.12 m_0 and 0.19 m_0 for the N content of 1 % and 2 %, respectively, in GaAsN/GaAs QWs. In Reference 9 a value of 0.4 m_0 was found for the effective mass in $Ga_{0.92}In_{0.08}N_{0.033}As_{0.967}$ with an electron concentration of 6×10^{19} cm^{-3}. An increase of the effective mass in the Ga(In)NAs alloys compared to Ga(In)As has also been predicted by different theories [9, 32, 33] described in section 2.2.

2.2 Theoretical models

Over the last few years a significant effort has been made to understand the physical origin of the unusually large effect of nitrogen on the electronic structure of III-V-N alloys. The first attempts by Sakai *et al.* [34] were based on a dielectric model that predicted highly nonlinear composition dependencies of the bandgap. The first-principle supercell calculations by Wei and Zunger [29] could only consider ordered alloys. Recent experimental discoveries have posed new challenges for band structure theories. A greatly reduced and strongly nonlinear pressure dependence of the bandgap has been measured in GaInNAs alloys [12, 13, 35]. A new optical transition around 1.8 eV has been found in photomodulated reflectance experiments [7, 13]. The notations E_- and E_+ originally proposed in [13] for the bandgap of GaInNAs and for this new optical transition are commonly used. Two groups of models, the band anticrossing model and the model based on pseudopotential theory, have recently been proposed to explain the conduction band structure and the origin of the N-induced E_- and E_+ bands.

The two-level band anticrossing model (BAC) describes the electronic structure of GaInNAs alloys in terms of an interaction between the localized state of nitrogen and the extended conduction band states of the host semiconductor matrix [13, 36], which results in splitting of the conduction band to the E_- and E_+ bands and a reduction of the fundamental bandgap. The E_+ transition is blueshifted and the E_- transition is redshifted from the N resonant level with increasing N concentration. The BAC model provides simple analytic expressions for the conduction band dispersion as a function of N concentration x and allows to calculate, for example, the strength of the optical transitions [37] in bulk materials and the transition energies between electronic states in QWs or the gain in laser structures [38]. The formula for the lower E_- and upper E_+ subband is given by

$$E_{\pm}(k) = \frac{1}{2}\left[\left(E_M(k) + E_N \right) \pm \sqrt{\left(E_M(k) - E_N \right)^2 + 4xC_{MN}^2} \right], \qquad (2)$$

where $E_M(k)$ is the energy of the conduction band of the semiconductor matrix, E_N is the energy position of the N-related level relative to the top of the valence band, x is the nitrogen molar fraction, and C_{MN} is the parameter describing the coupling between the two types of states. Well established values for the parameters E_N and C_{MN} are 1.65 eV and 2.7 eV, respectively, at the temperature of 300 K [39]. Figure 3 shows the conduction band splitting in $Ga_{0.96}In_{0.04}N_{0.01}As_{0.99}$ calculated according to equation 2. Parabolic approximation was used to describe the conduction band of GaInAs.

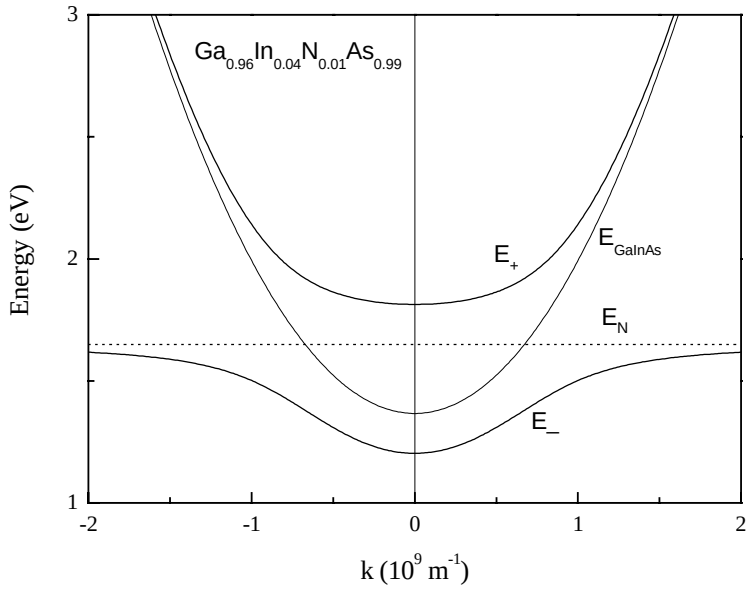

Figure 3. The conduction band structure of $Ga_{0.96}In_{0.04}N_{0.01}As_{0.99}$ near the Γ-point (k = 0) calculated with the BAC model. A parabolic approximation for the conduction band of GaInAs was used. The splitting of the conduction band into E_- and E_+ bands is clearly shown. The energy scale is relative to the top of the valence band.

Based on the dispersion relations a number of new effects, such as a N-induced increase of the electron effective mass [9] and improvement in the donor activation efficiency of GaInNAs alloys [40], have been predicted and experimentally confirmed. As shown in figure 3, the BAC model predicts a distinct flattening of the $E_-(k)$ dependence for the electron energies approaching E_N. This non-parabolic shape of $E_-(k)$ must lead to an increase of the effective mass. The BAC model has also been used to describe the pressure dependence of the interband transitions in GaPN and the Al composition dependence of the E_+ and E_- transitions in AlGaNAs alloys [41]. Most recently, it has been shown that the BAC model also applies to ZnSTe and ZnSeTe II-VI semiconductor alloys that exhibit large bandgap bowing parameters and strongly

nonlinear pressure dependencies of the bandgap [42]. A modified version of the BAC model including an interaction of the conduction and valence bands within the $\mathbf{k} \cdot \mathbf{p}$ approximation has also been proposed [43].

Besides the BAC model, other interpretations of the composition and pressure dependence of the bandgap of Ga(In)NAs have been proposed on the basis of local density approximation (LDA) and **empirical pseudopotential method (EPM)** calculations [31, 35, 44-50]. The EPM method enables the study of very large systems and is able to evaluate the electronic consequences of, for example, specified small clusters on the overall properties of an alloy. The method includes atomic relaxation, multi-band coupling and enables systems with up to 10^4 atoms to be studied (versus ~ 200 in LDA). The micro- and nanostructure of the studied system is described in EPM by generating supercells and distributing cations and anions at the corresponding atomic sites in these supercells.

Recent works [48-50] suggest that the properties of GaAsN and GaPN alloys can be analysed in terms of small localized nitrogen cluster states and delocalized perturbed host states. The EPM method differs from the BAC model which ignores cluster states beyond the isolated nitrogen and uses only a single host state. In EPM the E_- and E_+ bands originate from the mixing of the Γ, L, and X states of the host with only a minor contribution of the N state. Supercell calculations of small nitrogen clusters have shown that Ga-centered clusters with 2-4 nitrogen atoms can introduce very deep states having energy levels at about 200 meV below the conduction band minimum of GaAs. The localized cluster states remain fixed in energy with increasing N concentration. The edge of the conduction band minimum E_- moves rapidly to lower energies due to anticrossing and repulsion with higher energy members of the perturbed host states, and overtakes the discrete cluster states one by one. At a critical composition of x_c ~ 0.6 % in GaAs and x_c ~ 2 % in GaP the deepest cluster states are overtaken by the moving perturbed host states. The upper edge of the perturbed host states, E_+, appears for x > 0.6 % and moves up in energy with increasing N concentration. The use of the EPM methods for GaInNAs leads to the predictions that the bandgap will reach a zero value for large enough N concentrations (x ~ 20 %) [51].

2.3 Band alignment

It has been commonly accepted that nitrogen incorporation mainly affects the conduction band states of the Ga(In)NAs alloys leading to an increase in the conduction band offset and only a small discontinuity in the valence band edge. However, a debate has been going on regarding the fundamental type of the band alignment, shown schematically in figure 4. Early theoretical studies based on the dielectric model predicted type-II alignment for the GaAsN/GaAs system [34] in contrast to the more recent first-principles calculations [44] which suggest a type-I

band alignment. Contradictory results have also been obtained by experimental studies [52-57]. The reported valence band offsets also vary considerably. Due to the nonlinearity of the $GaAs_{1-x}N_x$ bandgap, the valence band offset ratios given in the literature are only valid for the corresponding *x*.

The most recent results strongly favor a type-I band alignment. In reference 56 the character of optical transitions, *i.e.*, direct in space for type-I versus indirect for type-II structures, was determined from time-resolved photoluminescence measurements. Identical radiative lifetime of the near-bandgap emission measured in the GaAsN/GaAs multiquantum well structures and single GaAsN epilayers indicated that optical transitions are direct in real space. In addition, magneto-optical studies supported a type-I band alignment. Similar conclusion has also been reached for the GaInNAs/GaAs structures based on the results from polarized photoluminescence excitation spectroscopy [57], as well as by analysing the effect of quantum confinement on the energies of optical transitions [11, 58, 59].

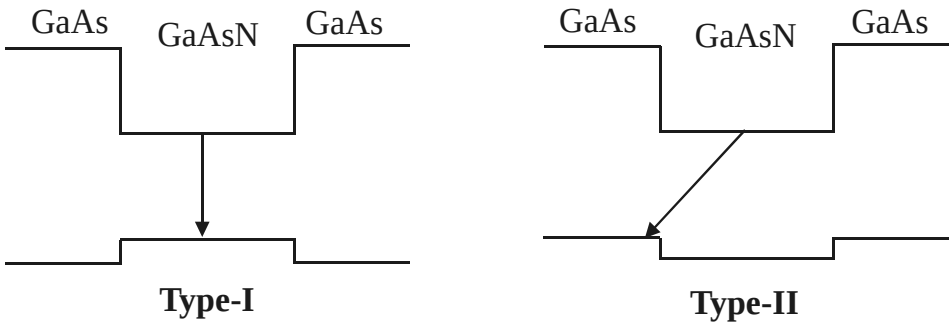

Figure 4. Schematic representation of band alignment in type-I and type-II quantum structures. The arrows show dominant recombination transitions, i.e., direct in space for type-I transitions and indirect in space for type-II transitions. Both band alignments have been proposed for GaAsN/GaAs quantum structures, but recent results strongly favor the type-I band alignment.

2.4 Device applications

The first continuous-wave long-wavelength GaInNAs laser on GaAs operating at room temperature was reported by Kondow *et al.* in 1996. The device was a broad area, single QW laser emitting at 1.18 μm with a threshold current density of 1.83 kA/cm^2. With significant development since that time, the threshold current densities have dropped dramatically and output powers have increased substantially. The main focus for GaInNAs edge-emitting lasers in the past 2-3 years has been to extend the wavelength beyond 1.3 μm. This has been done by using GaAsN barriers [60-62] and/or by adding antimony to the growth of the QW layers [63-67]. Ridge

waveguide lasers with GaInNAsSb QWs and GaAsNSb barriers operating at 1.465 μm have been reported [66, 67]. The threshold current density for these devices was 2.8 kA/cm^2. The lowest laser threshold current densities reported are 350 A/cm^2 for 1.3 μm single QW lasers [68].

The first VCSELs with an active region consisting of GaInNAs/GaAs QWs and emitting around 1.2 μm were also realized by Kondow *et al.* in 1998 [69]. Reflecting the problems of obtaining high-quality material emitting at longer wavelengths, the first GaInNAs-based VCSELs emitting at 1.28 μm or beyond were realized two years later [70, 71]. All these early VCSEL structures were grown by molecular beam epitaxy but more recently 1.3 μm VCSELs have been grown also by metalorganic vapor phase epitaxy [72-73]. Infineon Technologies has grown 1.3 μm VCSELs by both growth methods [68, 71, 73]. The devices are suitable for data transmission up to 10 Gbit/s with an bit error rate of less than 10^{-11}. The continuous-wave output power and threshold current of these devices are around 1 mW and 1-2 mA, respectively, at room temperature. These results promise that GaInNAs-based VCSELs will be suitable for data-link systems.

Following the introduction of GaInNAs as a 1 eV-bandgap semiconductor lattice-matched to GaAs, it was realized that GaInNAs could be a suitable material for multijunction solar cell designs and GaInNAs solar cells were demonstrated in laboratories [74, 75]. However, the short minority-carrier diffusion length in GaInNAs [76, 77] caused by low carrier mobilities [76, 77, 78] and short lifetimes [55, 79] imposes a serious problem for solar cell applications. For terrestrial operation conditions, the performance of today's GaInNAs solar cell junctions would have to be significantly improved even to reach the efficiency of the widely used GaInP/GaAs/Ge three-junction solar cell.

The use of GaInNAs can be beneficial in heterojunction bipolar transistors (HBTs). GaAs HBTs are in widespread use, especially in microwave power amplifiers for wireless applications. The use of GaInNAs in the base region of the HBTs allows a reduction of the turn-on voltage of the devices and facilitates their use in applications with low power supply voltage, particularly in battery operated power amplifiers for mobile communications. HBTs with GaInNAs base regions have been demonstrated successfully by different groups [80-82]. The major task is to verify the reliability of the devices before GaInNAs HBTs can be put into production.

3 EXPERIMENTAL TECHNIQUES

Metalorganic vapor phase epitaxy (MOVPE) was used to grow the epitaxial structures for this thesis. The main features of the method and the MOVPE apparatus are described in section 3.1. The techniques used to study the optical properties of the samples are presented in section 3.2. The surfaces of the QD samples were imaged with atomic force microscopy (AFM) which is described in section 3.3. X-ray diffraction, which was used to determine the composition and thickness of the grown epitaxial layers is described in section 3.4.

3.1 Metalorganic vapor phase epitaxy

In epitaxial growth techniques the atoms are attached to the substrate surface in such a way, that the crystal structure of the substrate is copied to the growing epitaxial layer. MOVPE growth technique was developed at the end of the 1960's [83]. The widely used synonyms of MOVPE are metalorganic chemical vapor deposition (MOCVD), OMVPE and OMCVD. The source materials are typically metalorganic and hydride compounds. The metalorganic compounds are usually liquids at room temperature, whereas the hydrides are gases. The source materials are mixed with a carrier gas and transported to a reactor having a substrate wafer on a heated susceptor. The precursors dissociate due to the elevated temperature above the susceptor [84], and the group-III and the group-V elements diffuse to the surface of the substrate. After the atoms are adsorbed to the surface, they can diffuse on the surface, nucleate into the growing epilayer or desorb away. MOVPE systems are nowadays capable of producing atomically sharp heterointerfaces with excellent uniformity over a number of wafers. Optical in-situ measurement techniques enable accurate surface temperature and growth rate measurements, which can be utilized to achieve more precise growth control.

The epitaxial structures studied in this thesis were grown with the MOVPE apparatus of Optoelectronics Laboratory at Helsinki University of Technology. The schematic representation of the system, manufactured by Thomas Swan Scientific Equipment Ltd., is shown in figure 5. All the group-III and group-V source materials in this system are metalorganic compounds. Trimethylgallium (TMGa) and trimethylindium (TMIn) are used as group-III sources for gallium and indium, respectively. The group-V precursors used in this work are tertiarybutylarsine (TBAs), dimethylhydrazine (DMHy) and tertiarybutylphosphine (TBP) for arsenic, nitrogen, and phosphorus, respectively. Hydrogen is used as the carrier gas. The source materials are held in steel bubblers in temperature-controlled baths. The carrier gas flows through the bubbler and is saturated with the source material. The concentration of the

precursor in the gas is determined by the vapor pressure of the compound in the bubbler at the bath temperature. The flow rate is controlled by mass flow controllers (MFCs).

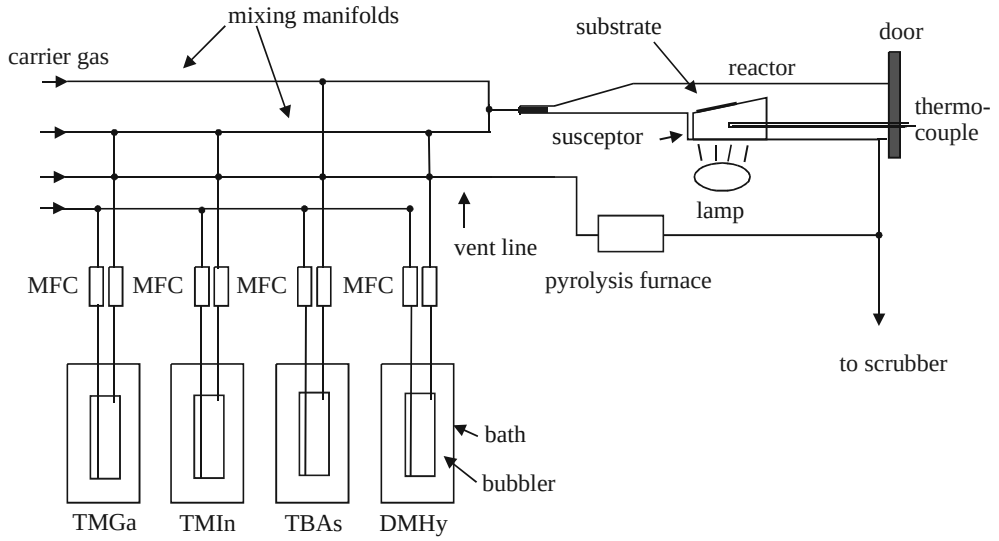

Figure 5. Schematic representation of the MOVPE apparatus.

Before the growth the output flows from the bubblers are directed continuously into the vent line bypassing the reactor in order to stabilize the flow rates and the concentrations. The vent line is directed through a pyrolysis furnace to the exhaust. The growth is initiated when the precursors are switched to the reactor lines. The flows are directed to separate mixing manifolds for the group-III and group-V precursors to reduce the probability of unwanted pre-reactions. However, DMHy is injected to the group-III mixing manifold due to the lack of proper connection to the group-V manifold. The time for the pre-reactions is still very short, because the carrier gas flow is quite high. The horizontal quartz reactor produces a laminal flow pattern over the susceptor having an area of about 5 cm^2. The reactor pressure can be controlled between about 20 mbar and atmospheric pressure, but all the structures for this thesis were grown at atmospheric pressure. The susceptor is heated by a halogen lamp and the temperature is measured by a thermocouple located inside the susceptor. All the temperatures mentioned in this thesis are thermocouple readings. The actual surface temperature of the substrate in a similar reactor at the temperature of 650 °C has been measured to be 50°C lower than the thermocouple reading due to the cooling effect of the flowing gas [85]. Behind the susceptor the gas flow is guided to the exhaust, where the unused components are absorbed and oxidized in a charcoal scrubber.

3.2 Optical spectroscopy

The optical properties of the samples were studied mainly by photoluminescence (PL) spectroscopy. PL is a widely-used, non-destructive spectroscopic characterization method which gives information about energy states and different radiative recombination channels in semiconductors. The photons from the excitation beam are absorbed by the sample and electron-hole pairs are created. The carriers thermalize quickly to the band edge through phonon emission, diffuse in the structure and recombine radiatively or non-radiatively. A typical PL spectrum is composed of several types of transitions. Common radiative transitions are a band-to-band transition, a transition from the conduction band to an acceptor state, and excitonic transitions. Two frequently used methods for identification of the different transitions are measurements as a function of temperature and excitation laser power. From temperature-resolved PL measurements the thermal activation energies of the transitions can be extracted and thus information about the energy states can be gained. The temperature dependence of the integrated PL intensity can be formulated as

$$I(T) = \frac{I_0}{1 + \sum_{i=1}^{n} c_i e^{-E_i / kT}}, \tag{3}$$

where c_i is a temperature-dependent parameter for each transition mechanism i, E_i is the corresponding thermal activation energy and I_0 is the intensity at T = 0 K [86].

The PL setup used in this thesis is presented in figure 6. An argon-ion laser with a wavelength of 488 nm was used for excitation. The laser light was guided with mirrors through a chopper and focused onto a sample attached to a cold finger of a closed-cycle helium cyostat. The cryostat can be cooled down to about 9 K. The luminescence emitted from the sample was focused with a lens to the input slit of the monochromator and dispersed with a grating of the monochromator. A germanium diode cooled with liquid nitrogen was used to detect the light intensity at a selected wavelength. The signal from the detector and the reference frequency obtained from the chopper were guided to a phase-locked amplifier. The data was collected by a computer connected to the monochromator and to the phase-locked amplifier.

For publication VII the decays of the different PL peaks were time-resolved. In the time-resolved PL measurements the sample was excited by 150 fs pulses at the wavelength of 800 nm from a mode-locked titanium-sapphire laser. Signal was detected by a microchannel plate photomultiplier and photon counting electronics. Temporal resolution of the system was 30 ps.

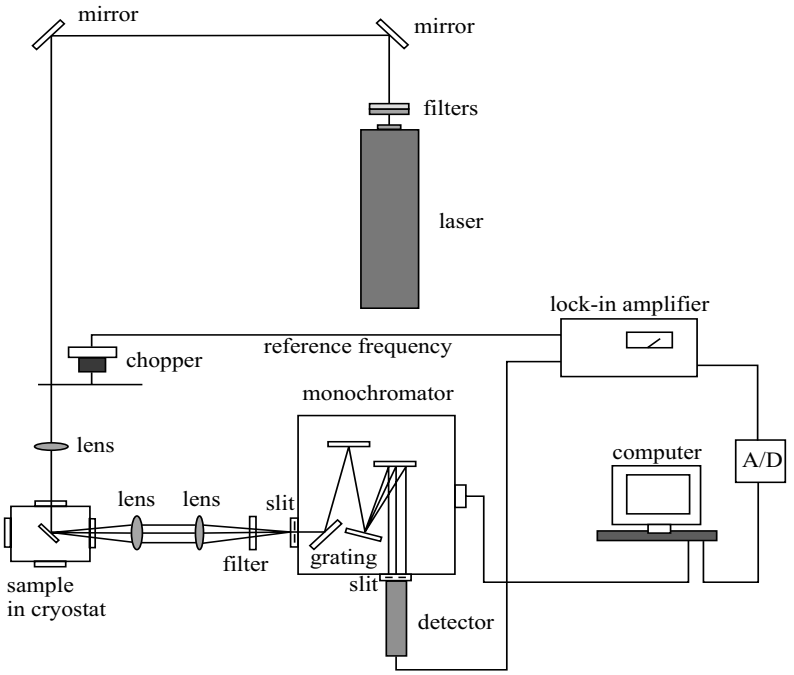

Figure 6. Schematic representation of the PL setup used in this work.

3.3 Atomic force microscopy

Atomic force microscopy (AFM) is one of the surface probe microscopic techniques in which a surface property, *e.g.*, morphology or charge density, measured by the probe is generated into an image by a computer. The operating principle of the AFM apparatus used in this work is schematically shown in figure 7. The sample is in close vicinity to a Si_3N_4 probe tip and a laser beam is reflected from the tip to the detector. When the tip bends according to the shapes of the sample surface, the signal of the detector changes. This signal is used to move the sample holder by piezoelectric actuators. The sample is scanned laterally and a feedback-loop is used to move the sample vertically in order to keep the tip at a fixed position. The voltage of the vertical piezo is converted to height information for image construction.

In this work a contact-mode AFM, Nanoscope E, was used to image surfaces of the QD samples in publications II, V and VII. The AFM measurement gives accurate information about the height and the areal density of the self-organized islands. The accuracy of the AFM apparatus is sufficient to resolve height differences of one monolayer, but due to the finite curvature of the AFM tip the generated image is a convolution of the shapes of the tip and the island [87]. The surface image given by the

AFM used in this work consists of 512 × 512 measurement points and the maximum measurement area is 13 × 13 μm^2. The images can be edited and analyzed using a computer software.

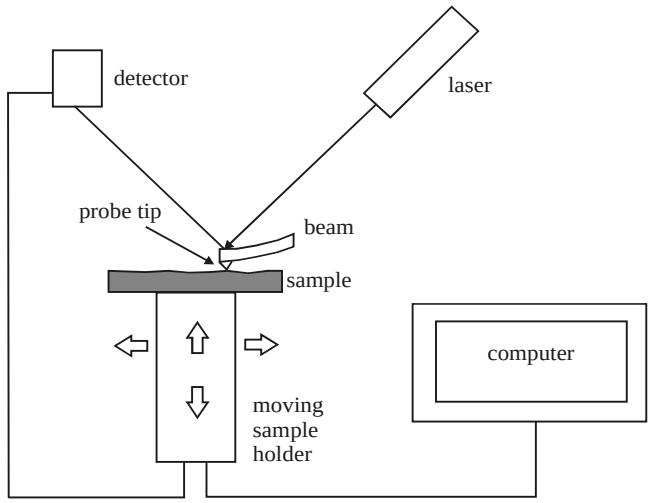

Figure 7. Schematic illustration of the operating principle of the AFM apparatus used in this work.

3.4 X-ray diffraction

The x-ray diffraction measurement used in this thesis is based on the diffraction of x-rays from the lattice planes of the crystalline sample. The angle of diffraction θ is dependent on the x-ray wavelength and distance between the lattice planes according to the Bragg's law [88]

$$\sin\theta = \frac{\lambda}{2d_{hkl}}, \tag{4}$$

where λ is the x-ray wavelength and d_{hkl} is the distance between the lattice planes given by

$$d_{hkl} = \frac{a}{\sqrt{h^2 + k^2 + l^2}}, \tag{5}$$

where a is the lattice constant and h, k and l are integers. Depending on the lattice structure of the sample, there may be no diffraction at all for some (hkl)-combinations.

Therefore, only certain (*hkl*)-combinations are usually allowed. For example, the diffraction maximum of GaAs is obtained from (400) diffraction. A diffraction curve is obtained by measuring the diffracted intensity as a function of the diffraction angle. The diffraction from the substrate is usually strong. If the lattice constant of the grown epitaxial layer is different than that of the substrate, the diffraction maximum of the epitaxial layer is observed at a different angle. In superlattice structures an interference pattern is observed instead of single peaks from different materials.

In this work a modular Philips X'Pert Pro high-resolution x-ray diffractometer was used to determine the thickness and composition of the grown epitaxial layers. Figure 8 shows a basic setup used for rocking curve measurements. X-rays are generated in an x-ray tube using Cu anode. A monochromator containing four Ge crystals is used to obtain a narrow-band Cu-Kα_1 x-ray beam at the wavelength of 1.541 Å. An x-ray mirror is placed between the x-ray generator and the monochromator to collimate the x-ray beam, which increases the intensity throughput of the monochromator. The sample is attached to a goniometer that positions the sample in the monochromatic x-ray beam with an incident angle ω between the beam and the surface of the sample. In this $\omega/2\theta$–measurement the incident angle ω deviates from the angle of diffraction θ by an offset angle, which depends on the positioning of the sample on the sample holder and on the possible miscut of the sample substrate. The x-ray diffraction from the sample is detected with a movable xenon/methane detector. The diffraction curves of epitaxial layers can be simulated using a software based on the dynamical theory of x-ray diffraction [89]. The layer thicknesses and compositions can be obtained by comparing measured and simulated curves.

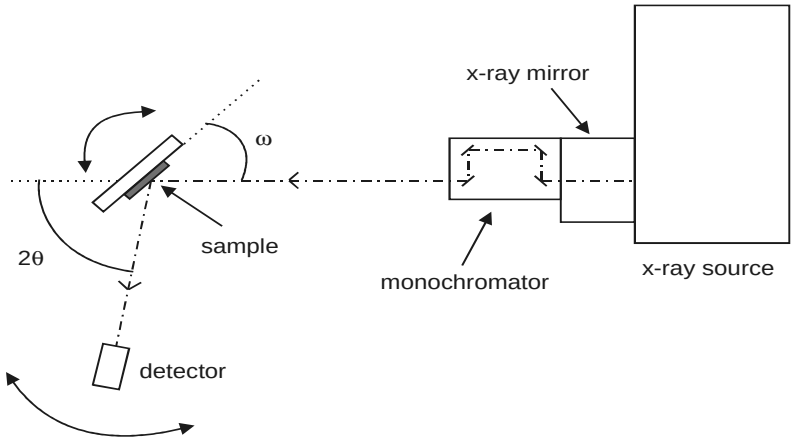

Figure 8. Schematic representation of the x-ray diffraction measurement setup. The angle between the incident beam and the sample surface is ω and the angle between the incident beam and the diffracted beam is 2θ.

4 BULK AND QUANTUM WELL STRUCTURES

This chapter discusses the results of publications I, III, IV, VI, and VIII. In these publications Ga(In)NAs bulk layers and QWs were studied. Section 4.1 presents the studies of the growth and annealing of GaAsN and GaInNAs structures. Section 4.2 discusses the dislocations and defects found in GaAsN bulk layers. Section 4.3 describes the effects of laser treatment on the optical properties of QWs.

4.1 Growth and annealing of Ga(In)NAs

The MOVPE growth of GaAsN and GaInNAs bulk and QW structures was studied in publications I and III. In publication I the growth conditions of GaAsN were optimized for N concentration of up to 5.6 %. The aim of the work for publication III was to reach 1.55 μm room-temperature luminescence on GaAs. Special growth conditions compared to earlier material systems are required for the growth of Ga(In)NAs. In order to incorporate sufficiently nitrogen, the growth has to be done at much lower growth temperatures ($T < 600$ °C) and under metastable growth conditions within the miscibility gap region of the alloy [61, 90]. Therefore, precursors should have low decomposition temperatures. The precursor used for gallium in this thesis, TMGa, decomposes incompletely at low temperatures. In publication III a decrease in the growth rate due to the incomplete TMGa decomposition was estimated to be 10 % at 540 °C and 15 % at 520 °C compared to the growth rate at higher temperatures.

The N concentration was found to decrease with increasing growth temperature. Figure 9 shows the N concentration as a function of the growth temperature for GaInNAs multiple quantum well (MQW) structures with In compositions of 10 and 30 %. The rapid decrease of the N concentration with increasing growth temperature is probably caused by the temperature enhanced N desorption from the surface. The maximum N concentration is obtained at 520 °C. Decreasing the growth temperature further results in poor crystal quality. Figure 9 also shows that in the MOVPE growth of GaInNAs with DMHy and TMIn precursors the nitrogen incorporation is significantly reduced as the In concentration is increased [26, 74]. The cause of this effect is not completely understood yet, but enhancement of indium surface segregation has been proposed as a possible reason [74]. Other nitrogen sources, including hydrazine [91], t-butylhydrazine [92] and NF_3 [92, 93], have been found to incorporate nitrogen more efficiently than DMHy. On the contrary to the hydrazine-type sources, layers grown with NF_3 show only a minimal dependence of the nitrogen content on the In concentration [92]. These results do not support indium surface segregation as a reason for the reduced nitrogen incorporation.

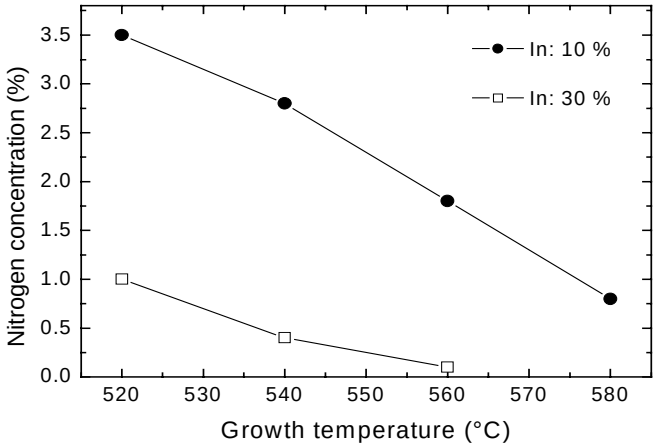

Figure 9. Effect of growth temperature on the N concentration for In concentrations of 10 and 30 % in GaInNAs MQW structures.

Figure 10 shows the effect of the DMHy/TBAs ratio on the N concentration of the GaAsN layers grown at 530 °C. At low growth temperatures a low TBAs/III ratio of about two is sufficient for the surface protection of GaAsN. When the TBAs flux is kept constant (TBAs/III = 2), the N concentration increases linearly with increasing DMHy flux up to 5 % and then saturates to 5.6 %. The dependence of the N concentration on the TBAs flux is also linear, the N concentration increases with decreasing TBAs/III ratio. However, when the TBAs/III ratio was decreased below 2, no high-quality crystal growth was observed because the surface protection was lost. The N concentration becomes more and more sensitive to the V/III ratio with increasing DMHy/V ratio. In order to incorporate over 2 % of nitrogen into GaAs, more than 80 % of the total group-V gas flow has to be DMHy. In publication III large DMHy/V ratios of up to 0.97 were used to overcome the reducing effect of indium on the nitrogen incorporation.

In publication III it was found that there exists an optimum growth window at the In concentration of around 23 %, where the smallest PL peak energies are achieved. Figure 11 shows the low-temperature PL data from GaInNAs MQW samples grown with the In composition of 22.8 %. As expected, the PL peak energy decreases from 1.277 eV to 0.821 eV when the N concentration is increased from 0 to 3.7 %. The PL intensity of Ga(In)NAs is known to decrease rapidly with increasing N concentration [26, 74]. This is due to the various defects and non-radiative recombination centers which have been observed to form during the growth process [94-98]. The PL intensity of the sample grown with the N concentration of 2 % is about three orders of magnitude smaller than that of the $GaIn_{0.228}As$ reference sample. However, further increase in the N concentration does not result in such a drastic decrease of the PL intensity. The full width at half maximum (FWHM) of the PL peaks increases from

23 meV to 56 meV, which indicates increased alloy disorder with increasing N concentration.

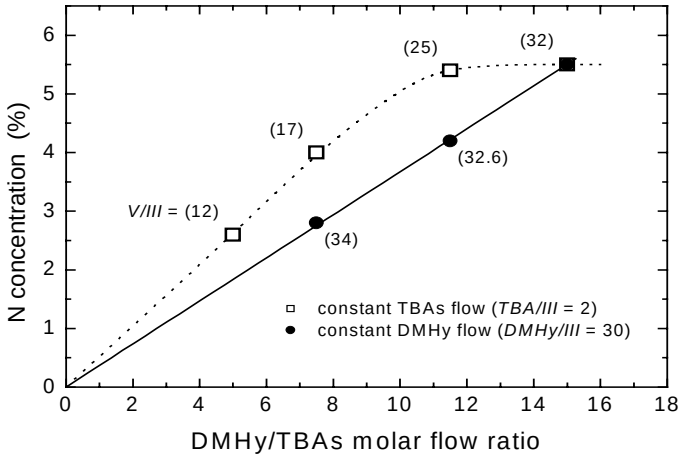

Figure 10. Effect of DMHy/TBAs ratio on the N concentration of GaAsN layers. The V/III ratio of each sample is shown in parentheses.

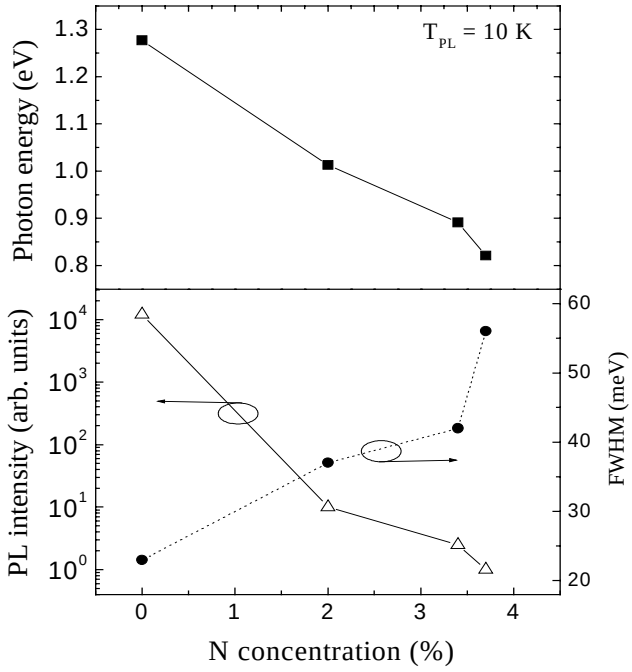

Figure 11. Low-temperature PL data from $Ga_{0.778}In_{0.228}N_xAs_{1-x}$ MQW structures as a function of the N concentration. The PL peak energy and the PL intensity decrease and the FWHM increases with increasing N concentration.

It was soon observed that the PL intensity of Ga(In)NAs structures could be increased by thermal annealing [99]. However, annealing results also in a strong blueshift of the emission wavelength. Several annealing studies have been published yielding somewhat contradictory results [96, 99-104], which is partly due to the different annealing and growth conditions used but also shows the metastability of this material system. In publications I and III in-situ and post-growth annealing cycles were performed in the MOVPE reactor under excess arsenic ambient and the optical properties of the annealed structures were investigated. No difference between the two annealing methods was observed. Figure 12 shows the effect of 10 min post-growth annealing at different temperatures on the PL peak energy and intensity of a GaInNAs MQW structure. Annealing at 700 °C increases the PL intensity by a factor of 300. The enhancement of the PL intensity is most likely due to the reduction of non-radiative centers [96]. Further increase of the annealing temperature results in thermal generation of new non-radiative defects and thus decrease of the PL intensity.The PL peaks blueshift for all annealing temperatures.

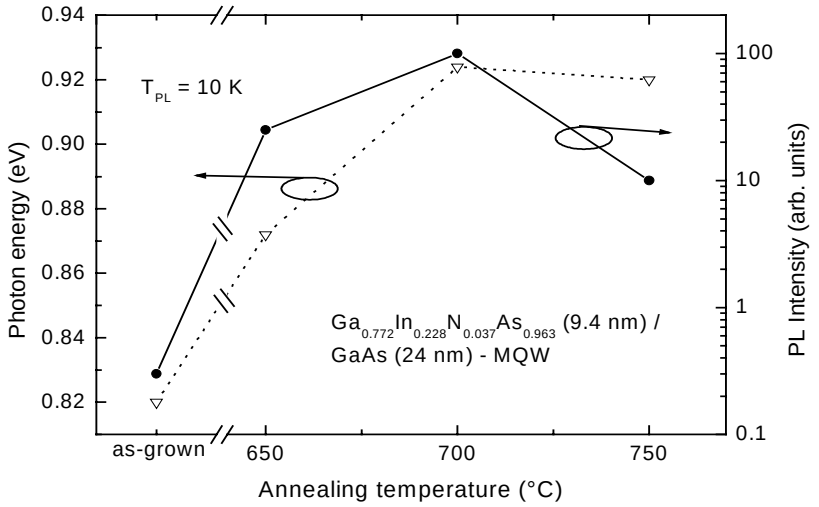

Figure 12. PL peak energies and intensities of a MQW structure after post-growth annealing at different temperatures for 10 min. The PL peaks blueshift for all annealing temperatures. The PL intensity is increased over two orders of magnitude by annealing at 700 °C.

Different mechanisms causing the blueshift of the bandgap, such as nitrogen outdiffusion [96] and Ga-In interdiffusion [105], have been suggested. Recently, local rearrangement of the neighboring atoms of nitrogen has been proposed to explain the blueshift [106]. It has been found that in as-grown GaInNAs the nitrogen atoms are mainly bonded to four gallium atoms and after annealing nitrogen atoms have one or more bonds with indium atoms [107, 108]. In publication III it was also found that

annealing for longer times than 10 min does not result in further enhancement of the PL intensity but increases the blueshift of the PL peak. Therefore, the optimum annealing condition regarding the PL intensity is 10 min at 700 °C. Low-temperature PL wavelength of 1.61 μm was obtained from a $Ga_{0.74}In_{0.26}N_{0.03}As_{0.97}$ MQW structure. After annealing the PL wavelength of 1.51 μm was obtained at room temperature.

4.2 Defects and dislocations in GaAsN

Various defects are formed in the Ga(In)NAs material during the growth process. Intrinsic point defects identified in the arsenide-nitrides so far are an As_{Ga} antisite [94, 95], an N interstitial [96-98], and a gallium vacancy [98]. Some of the defects can be eliminated by post-growth annealing. In publication IV positron annihilation spectroscopy [109] was used to study vacancy-type defects in 170-nm-thick GaAsN epitaxial layers and the effect of annealing on the vacancy density was studied. The presence of vacancy defects in MOVPE-grown GaAsN was detected and the defects were identified as gallium vacancies. The vacancies in the samples grown at > 500 °C probably belong to defect complexes with some other defects such as As_{Ga} or N_{Ga} antisites, because isolated gallium vacancies are not stable at temperatures above 300 °C [110].

Figures 13 (a) and (b) show the experimental gallium vacancy concentration and the PL intensity at 10 K of the GaAsN samples before and after annealing, respectively. The vacancy concentration increases with the N concentration up to the order of 10^{18} cm^{-3} and anticorrelates with the PL intensity. Annealing at 700 °C for 10 min under H_2 carrier gas flow and TBAs excess ambient reduces the vacancy concentration by a factor of five compared to that found in as-grown material. The anticorrelation of the gallium vacancy concentration and the PL intensity suggests that the defect complexes containing gallium vacancies may act as non-radiative recombination centers in GaAsN. Since the decrease of the PL intensity with increasing N concentration is very drastic, other non-radiative mechanisms are most likely present and contribute to the decrease of the PL intensity.

In order to grow high quality strained GaAsN epilayers on GaAs, it is important to know the critical thickness of misfit dislocation formation for the material system. In publication VI highly strained GaAsN epilayers were grown on GaAs and studied by synchrotron x-ray topography [111] and other measurement techniques. X-ray topography is sensitive to the strain caused by a dislocation, thus single dislocations can be identified in the images. The critical thickness of misfit dislocation formation for a $GaAs_{0.965}N_{0.035}$ layer on GaAs was observed to be between 50 and 80 nm. Post-growth annealing had negligible effect on dislocation formation. When the layer thickness was increased to 220 nm a few broad white lines indicating cracks appeared in the images. The cracks are expected to originate from the GaAsN-GaAs interface.

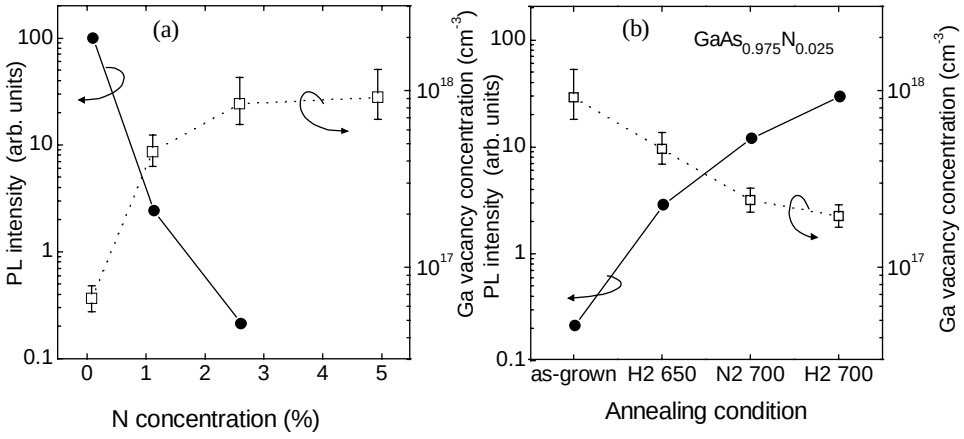

Figure 13. Gallium vacancy concentration and PL intensity of 170-nm-thick GaAsN epilayers as a function of (a) N concentration and (b) annealing condition. The lines are guides to the eye. The gallium vacancy concentration anticorrelates with the PL intensity

4.4 Effect of laser treatment on optical properties of QWs

The luminescence efficiency of the as-grown GaAsN QWs is small. In addition to the post-growth thermal annealing described in section 4.1, the luminescence intensity can be increased by laser treatment [99]. The laser treatment procedure has not been studied extensively, perhaps because it can be focused only to a part of a wafer at time, whereas thermal annealing of whole wafers is easy. However, a systematic study of laser treatments may reveal some new information about the optical properties and defects of the Ga(In)NAs alloys. Therefore, the effects of laser irradiation on the optical properties of 5-nm-thick GaAsN and GaInNAs QWs were studied in publication VIII.

Laser treatment was found to affect the GaAsN QWs quite similarly as thermal annealing. The most intense PL is obtained by utilizing both thermal and laser treatments. The effects of laser treatments were observed to be irreversible and local, *i.e.*, no degradation of the PL efficiency was observed even hours after the treatment and the efficiency was increased only in the area of the laser spot. In quaternary GaInNAs, the effects of thermal annealing and laser treatment differ from each other. Figure 14 shows PL spectra measured at 15 K from a $Ga_{0.8}In_{0.2}N_{0.02}As_{0.98}$ QW structure before and after both thermal annealing and laser treatment. As-grown GaInNAs shows reasonable PL intensity and, therefore, the effect of laser treatment is not as pronounced as in GaAsN. Laser treatment increases the intensity by a factor of 2.5 and

the blueshift of the PL peak is negligible. Thermal annealing causes a 10-fold increase in the PL intensity but shifts the PL peak by 86 meV to higher energies. Laser treatment has no impact on the optical properties of a thermally annealed GaInNAs sample.

Laser treatment enhances only the PL intensity of the QW peak, especially in the case of a GaAsN QW. Thus, the defect affected by the laser treatment is related to the layer containing nitrogen. When GaInNAs is annealed, the local configuration around a nitrogen atom changes [106] and the defect in question disappears. The laser treatment procedure affects the defects likely due to recombination-enhanced defect reaction [99, 112]. When pairs of electrons and holes are recombined within a short period of time through a non-radiative defect, the bandgap energy is transformed into lattice vibration energy by a series of coherent carrier captures. This reaction affects only one specific defect associated with a high non-radiative recombination rate. Laser irradiation could offer advantages in the cases like long-wavelength structures, where the blueshift of the PL peak should be avoided. Nevertheless, the laser treatment effects should be taken into account when measuring the optical properties of Ga(In)NAs samples.

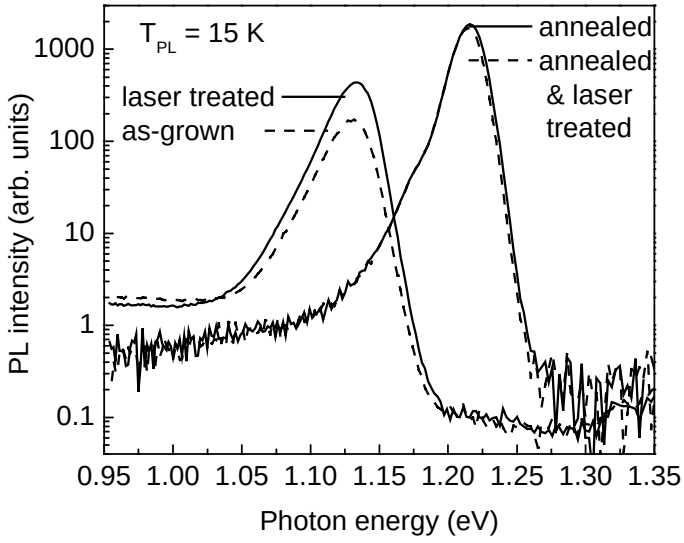

Figure 14. PL spectra measured at 15 K before and after thermal annealing and laser treatment of a $Ga_{0.8}In_{0.2}N_{0.02}As_{0.98}$ QW structure. The PL excitation and the laser treatment intensities were 42 W/cm^2 and 10000 W/cm^2, respectively.

5 QUANTUM DOT STRUCTURES

This chapter presents the discussion of the fabrication and the optical properties of GaInNAs QD structures studied in publications II, V, and VII. The fabrication of GaIn(N)As QDs on GaAs is described in section 5.1. The use of GaInNAs as a barrier material for GaInAs QDs and its effect on the QD emission wavelength is presented in section 5.2. Section 5.3 discusses the optical properties of GaInNAs QDs induced by the strain of InP islands.

5.1 Fabrication of GaIn(N)As QDs

Laser emission on GaAs at the wavelength of 1.3 μm can be realized by using self-assembled InAs or GaInAs QDs in the active region [113-117]. After the proposal of GaInNAs as a material for long-wavelength emission on GaAs, considerable effort has been devoted mainly to material and device research of GaInNAs QW lasers. However, GaInNAs can also be used to fabricate QD structures, and room-temperature PL at 1.52 μm has been reported from GaInNAs QDs grown by gas-source molecular beam epitaxy (MBE) [118]. GaInNAs QDs have also been grown by chemical beam epitaxy [119]. In publication II self-assembled GaIn(N)As QDs were grown by MOVPE and the effect of nitrogen on the formation and optical properties of the GaIn(N)As islands was investigated. Nitrogen in GaIn(N)As is shown in parentheses since the measurement of the actual N concentration in the QDs is very difficult.

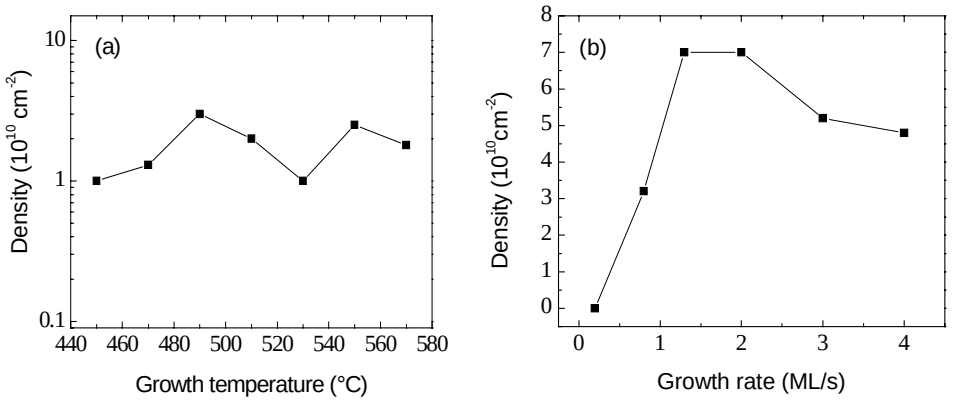

Figure 15. Island density of $Ga_{0.4}In_{0.6}(N)As$ samples as a function of (a) growth temperature and (b) growth rate.

For InAs and GaInAs QDs, it has been reported that the increase of growth temperature or the decrease of growth rate results in the increase of the dot size and the decrease of the dot density due to the increase of the migration length of the indium adatoms [120-122]. However, this behavior is somewhat different for GaIn(N)As QDs. Figure 15 (a) shows the dependence of the island density on the growth temperature for nominally 3.5-ML-thick $Ga_{0.4}In_{0.6}(N)As$ samples. As the growth temperature is increased from 450 °C to 570 °C the island density varies in the range of 1×10^{10}–3×10^{10} cm^{-2} and no clear tendency is observed. The average height of the islands varies between 5 and 10 nm. Figure 15 (b) shows the island density as a function of growth rate for nominally 4-ML-thick $Ga_{0.4}In_{0.6}(N)As$ samples. The island density is observed to be highest within the growth rate range of 1.3–2 ML/s. When the growth rate is decreased below 1 ML/s the island density decreases and no islands are formed with the growth rate of 0.2 ML/s probably due to increased desorption of the reactive species from the growth surface. Although this behavior is quite similar to the In(Ga)As islands, the average island height, however, remains almost constant at around 5 nm.

Figure 16 (a) shows an AFM image from a 4.5 ML $Ga_{0.4}In_{0.6}(N)As$ QD sample. The areal density and the average height of the islands are 5×10^{10} cm^{-2} and 5 nm, respectively. An AFM image from a reference $Ga_{0.4}In_{0.6}As$ sample grown without DMHy flow is shown in figure 16 (b). The island density in this N-free sample is smaller (2×10^{10} cm^{-2}) and the islands are higher on average (8 nm) compared to the sample grown with DMHy flow. This is in contrast to the results that were observed for MBE growth [118]. The reason for the larger dot density and smaller size of GaIn(N)As QDs could be related to the migration length of adatoms. Makino *et. al.* [119] have suggested that the nitrogen atom may change the surface potential due to its strong bond and decrease the migration length on the surface.

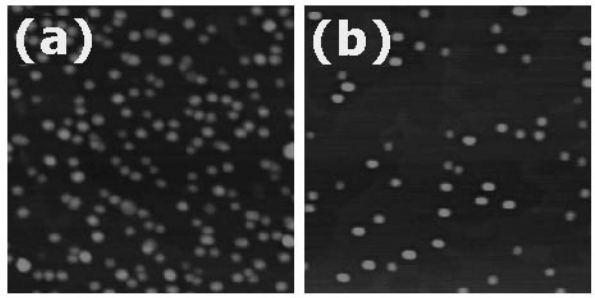

Figure 16. AFM images taken from QD samples grown at 530 °C with (a) 4.5 ML $Ga_{0.4}In_{0.6}(N)As$ and (b) 4.5 ML $Ga_{0.4}In_{0.6}As$. The scan size is 0.5×0.5 μm^2.

PL studies of the overgrown QD samples showed that the PL peak of the $Ga_{0.4}In_{0.6}As$ reference sample was actually at smaller energies compared to the sample

grown with DMHy flow. This indicates that a negligible amount of nitrogen is incorporated into the islands. The energy difference is explained by the larger average height of the $Ga_{0.4}In_{0.6}As$ islands. The reason for the negligible incorporation of nitrogen lies behind the large In concentration of the islands (see section 4.1). Figure 17 shows the dependence of the island density and the average island height on the DMHy/TBAs ratio for $Ga_{0.55}In_{0.45}(N)As$ QD samples with a coverage of 8 ML. The island densities in the $Ga_{0.55}In_{0.45}(N)As$ QD samples are significantly larger compared to the $Ga_{0.55}In_{0.45}As$ reference sample for all the used DMHy/TBAs ratios. Thus, by using DMHy during the island growth the island density can be increased by one order of magnitude. On the other hand, the island size can be varied to some extent by changing the DMHy/TBAs ratio. PL studies of overgrown islands indicate that the incorporation of nitrogen is still negligible. However, an enhancement of the 1.3 μm room-temperature luminescence by a factor of about three was observed in the $Ga_{0.55}In_{0.45}(N)As$ QD samples grown with DMHy flow. Thus, by introducing DMHy during the island growth the optical properties of the GaIn(N)As islands can be improved.

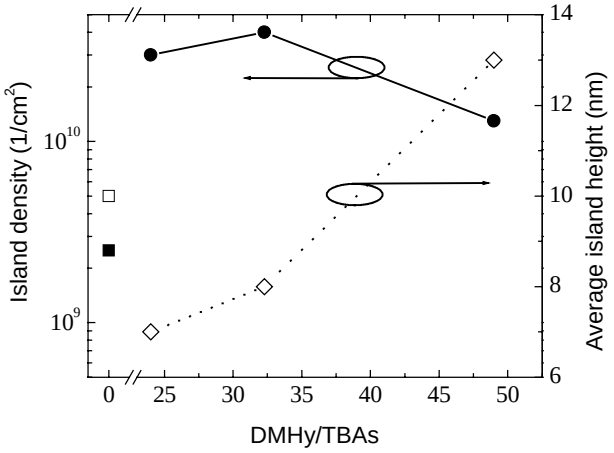

Figure 17. Island density and average island height as a function of DMHy/TBAs ratio for nominally 8-ML-thick $Ga_{0.55}In_{0.45}(N)As$ QD samples. The squares show the respective data for the reference $Ga_{0.55}In_{0.45}As$ QD sample.

5.2 Wavelength extension of GaInAs QDs

The transition energy of InAs or GaInAs QDs can be lowered and tuned to reach the 1.3 μm light emission by embedding the islands in an GaInAs QW, which leads to lower quantum confinement and reduced strain in the QDs [117, 123-125]. Since the nitrogen incorporation into GaInNAs QDs was found to be problematic in publication

II (see section 5.1), it could be more beneficial to use GaInAs as the QD material and bury them in GaInNAs. Therefore, self-assembled $Ga_{0.5}In_{0.5}As$ QDs embedded in GaInNAs were grown in publication V. The effect of the composition of the barrier layer on PL properties of the structures was investigated. A schematic illustration of the sample structure is shown in figure 18. The areal density of the islands was determined by AFM to be 2.4×10^{10} cm^{-2}. Since the growth conditions of the islands were not completely optimized, two types of small islands having an average height of 5 and 8 nm were observed.

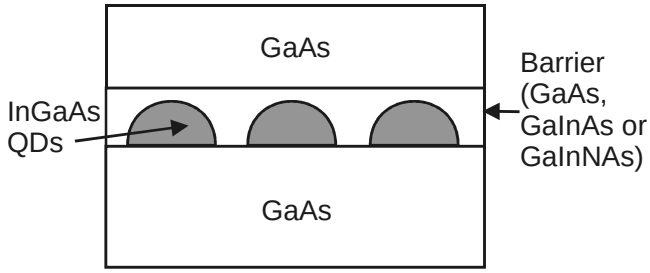

Figure 18. Schematic illustration of the $Ga_{0.5}In_{0.5}As$ QDs grown on GaAs and embedded in a $Ga_{1-y}In_yN_xAs_{1-x}$ barrier layer with different compositions. The In and N concentrations were varied in the range of $0 \leq y \leq 0.25$ and $0 \leq x \leq 0.035$, respectively. The thickness of the barrier layer was either 5 or 10 nm.

The use of GaInAs as a barrier layer was studied first and compared to the conventional GaAs cover. Since the lattice constant of the GaInAs barrier increases with increasing In concentration, the strain in the QDs is partly reduced due to the relaxation of the lattice constraint in the growth direction. This together with the decrease of the in-plane potential barrier height leads to the increase in the PL wavelength. By using a 5-nm-thick $Ga_{0.8}In_{0.2}As$ barrier the room-temperature PL wavelength was extended from 1.27 up to 1.42 μm and the PL intensity was increased by a factor of three compared to the conventional GaAs cover.

The GaInAs QDs were next covered by a 10-nm-thick $Ga_{0.85}In_{0.15}NAs$ layer. The N concentration was increased by increasing the DMHy/TBAs ratio. Figure 19 shows the development of the PL wavelength and intensity of the larger QDs as a function of the DMHy/TBAs ratio. As the embedding material is changed from GaAs to $Ga_{0.85}In_{0.15}As$, the PL peak redshifts and the intensity increases. As nitrogen is introduced into the barrier the PL peak redshifts first further, but then remains at the same wavelength up to a DMHy/TBAs ratio of 19. Although the N concentration of the barrier layer increases, this is not sufficient enough to shift the PL peak. The PL intensity increases slightly and stays higher than that obtained with the GaAs cover until the DMHy/TBAs ratio is increased to over 20. Further increase in the DMHy/TBAs ratio results in type-II band alignment when the conduction band edge of

the barrier material drops below that of the strained $Ga_{0.5}In_{0.5}As$ QDs. The PL peak redshifts, the intensity drops drastically, and the linewidth of the PL peak increases when the recombination occurs between electrons in the barrier material and holes in the $Ga_{0.5}In_{0.5}As$ QDs. Thus, by using a N-containing barrier layer an increase in the PL wavelength and intensity in the 1.3 μm wavelength range is observed.

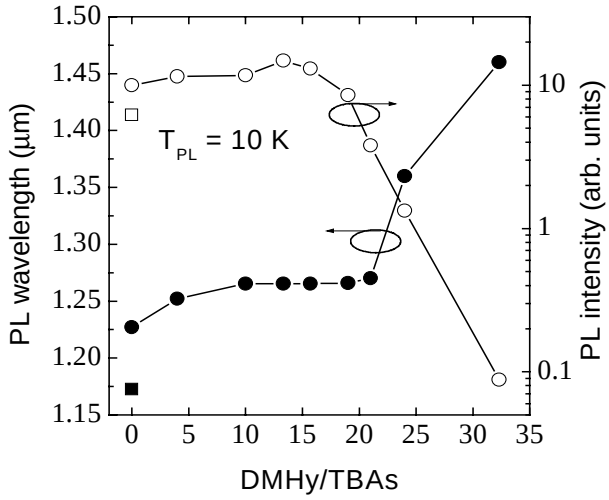

Figure 19. Dependence of the PL wavelength and intensity of the QDs on the DMHy/TBAs ratio used in the growth of the barrier layer. The squares show the respective data for QDs embedded in GaAs.

5.3 Strain-induced GaInNAs QDs

In publication VII strain-induced GaInNAs QDs were fabricated by using self-organized InP stressor islands grown on top of a GaInNAs QW. The use of self-organized islands as stressors was first demonstrated by Sopanen *et al.* [126]. Figure 20 shows schematically the sample structure and the formation of a strain-induced QD under an InP island. A 8-nm-thick $Ga_{0.8}In_{0.2}N_xAs_{1-x}$ QW and a 5-nm-thick GaAs barrier layer were grown on a 100-nm-thick GaAs buffer layer. Thermal annealing was performed to enhance the optical properties of the GaInNAs QW. After annealing a 5-nm-thick GaAs cap layer was grown and then an InP layer with a nominal thickness of 3 ML was fabricated. The growth mechanism of InP on GaAs is the coherent Stranski-Krastanow growth [127], where self-organized InP islands are formed. These islands act as stressors inducing a lateral parabolic QD potential in the QW due to tensile strain. This lateral potential together with the vertical QW confinement add up to a three-dimensional confinement potential. Therefore, a QD is formed into the QW

under the InP island. The base diameter and the height of the InP islands were measured by AFM to be about 100 and 20 nm, respectively. The measured base diameter depends on the shape of the AFM tip and is in reality less than 100 nm. The island density was about 1-2×10^9 cm^{-2} and the N concentration of the QWs was varied from 0 to 1.3 %.

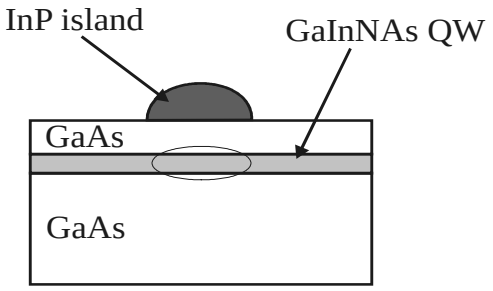

Figure 20. Schematic representation of the strain-induced GaInNAs QD sample. The InP islands act as stressors inducing a lateral parabolic QD potential in the QW. A QD is formed into the GaInNAs QW under the InP island.

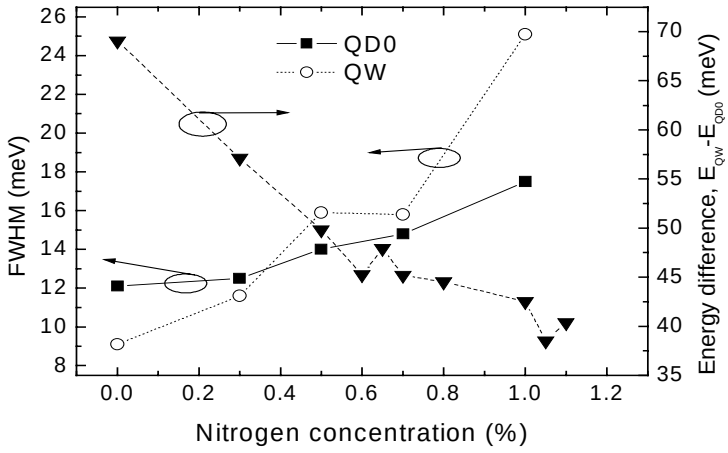

Figure 21. FWHM of the low-temperature (10 K) QW and QD0 PL peaks as a function of the N concentration of the QW. The energy difference of the PL peaks is also shown.

Low-temperature PL studies of the samples with increasing N concentration showed that the PL peaks of the samples containing nitrogen were broader and fewer excited states, typically only one, were seen compared to the nitrogen-free sample. A redshift of about 200 meV for the QW and QD peaks was observed as the N composition was increased from 0 to 1 %. Figure 21 shows the FWHM of the QW and QD ground state (QD0) PL peaks as a function of the N concentration. The energy separation between the QW and QD0 PL peaks is also shown. The FWHM of the QW

peak increases from 9 meV to 25 meV when the N concentration is increased from 0 to 1 %. Since the recombination linewidth of a single QD is very narrow, the broadening is probably due to composition or thickness variations in the QWs containing nitrogen. However, the FWHM of the QD0 peak is not as strongly affected by nitrogen. The lateral variation in the composition or thickness may take place in the scale of less than the diameter of the QDs (about 50 nm), because the QD peaks would otherwise broaden similarly to the QW peak. The energy difference of the PL peaks decreases from 69 meV for the nitrogen-free sample to about 40 meV for N composition of about 1 %. Carrier localization into states located few tens of meV below the band edge of the QW [128, 129] could explain such a decrease in the energy difference. The carrier localization can be explained by the potential minima originated from the composition and thickness fluctuations in the QW.

6 SUMMARY

The study of III-V-N alloys, especially GaInNAs, has been increasing in the last few years driven by the potential applications in laser and other devices for optical communications. Although the first commercial products utilizing GaInNAs are about to emerge on the market, challenges still remain in the understanding of the growth and the physics of the compound. The long-wavelength emission on GaAs substrates has also motivated the study of QD structures. In this work, Ga(In)NAs bulk, QW, and QD structures were fabricated on GaAs by MOVPE, and the composition of the samples was determined by x-ray diffraction measurements. The surface morphology of the QD structures was investigated with AFM. PL spectroscopy was used to investigate the optical properties of the structures.

The N incorporation efficiency into GaAs is very low and carefully optimized growth conditions are required to achieve N concentrations of over 4 %. The N concentration of the grown structures was strongly dependent on the growth temperature and the molar flow ratios of the different precursors, especially the DMHy/TBAs ratio. The growth conditions of GaAsN were optimized for high N concentration of up to 5.6 %. For GaInNAs/GaAs QW structures it was observed that the increase in the In concentration results in the decrease of the N concentration. Therefore, it is even more difficult to reach the technologically important 1.55 μm emission wavelength. In this work an optimum growth window at the In concentration of around 23 % was found for the longest emission wavelengths and a luminescence wavelength of 1.61 μm was observed from a $Ga_{0.74}In_{0.26}N_{0.03}As_{0.97}$ QW structure.

The optical properties of the as-grown structures deteriorate rapidly with increasing N concentration. Therefore, in-situ and post-growth thermal annealing procedures were used and optimized to enhance the optical quality. The enhancement of the luminescence intensity due to annealing was typically of the orders of magnitude. The optimum relation between the annealing temperature and the annealing time was found to be 10 min at 700 °C, and a room-temperature PL wavelength of 1.51 μm was observed from a $Ga_{0.74}In_{0.26}N_{0.03}As_{0.97}$ QW structure after post-growth annealing. Post-growth laser treatment was found to affect GaAsN QWs quite similarly to thermal annealing. However, for the GaInNAs QWs no blueshift of the PL peak was observed after the laser treatment in contrast to thermal annealing. Thus, laser treatment could offer advantages over annealing in the long-wavelength structures, where the blueshift of the PL peak should be avoided.

In order to grow material with good optical properties it is important to have information about the structural quality of the fabricated structures. GaAsN epilayers were shown to contain gallium vacancies in defect complexes. The anticorrelation of the vacancy concentration and the PL intensity suggests that these vacancy complexes may act as non-radiative recombination centers in GaAsN. One has to get rid of these vacancies and defects in order to improve the optical quality of the material. Highly-

strained GaAsN layers were studied by synchrotron x-ray topography and the critical thickness for misfit dislocation formation of the $GaAs_{0.965}N_{0.035}$ epilayer was found to be between 50 and 80 nm.

The incorporation of nitrogen from DMHy into self-assembled GaIn(N)As QDs was found to be negligible due to the high In concentration needed for island formation. It should be investigated whether more nitrogen could be incorporated into the islands by using other nitrogen sources. However, the use of DMHy during the growth was found to be useful, because the size and the areal density of the self-organized GaIn(N)As islands can be controlled and the optical properties improved by varying the DMHy flow. Although the 1.55 μm QD emission was not achieved, an enhanced room-temperature PL was observed at 1.3 μm wavelength from the QD samples grown with DMHy. On the other hand, the luminescence wavelength of GaInAs QDs can be extended and the PL intensity increased in the 1.3 μm wavelength range by embedding the islands in a GaInNAs barrier layer. Also strain-induced GaInNAs QDs were fabricated using InP islands as stressors.

REFERENCES

[1] M. Kondow, K. Uomi, A. Niwa, S. Watahiki, and Y. Yazawa, Japan. J. Appl. Phys. **35**, 1273 (1996).

[2] M. Weyers, M. Sato and H. Ando, Japan. J. Appl. Phys. **31**, L853 (1992).

[3] T. Makimoto, H. Saito, T. Nishida, and N. Kobayashi, Appl. Phys. Lett. **70**, 2984 (1997).

[4] G. Pozina, I. Ivanov, B. Monemar, J. V. Thordson, and T. G. Andersson, J. Appl. Phys. **84**, 3830 (1998).

[5] W. G. Bi and C. W. Tu, Appl. Phys. Lett. **70**, 1609 (1997).

[6] M. Kondow, K. Uomi, K. Hosomi, and T. Mozume, Japan. J. Appl. Phys. **33**, L1056 (1994).

[7] J. D. Perkins, A. Mascarenhas, Y. Zhang, J. F. Geisz, D. J. Friedman, J. M. Olson, and S. R. Kurtz, Phys. Rev. Lett. **82**, 3312 (1999).

[8] P. J. Klar, H. Grüning, W. Heimbrodt, J. Koch, F. Höhnsdorf, W. Stolz, P. M. A. Vicente, and J. Camassel, Appl. Phys. Lett. **76**, 3439 (2000).

[9] C. Skierbiszewski, P. Perlin. P. Wisniewski, W. Knap, T. Suski, W. Walukiewicz, W. Shan, K. M. Yu, J. W. Ager , E. E. Haller, J. F. Geisz, and J. M. Olson, Appl. Phys. Lett. **76**, 2409 (2000).

[10] P. N. Hai, W. M. Chen, I. A. Buyanova, H. P. Xin, and C. W. Tu, Appl. Phys. Lett. **77**, 1843 (2000).

[11] Z. Pan, L. H. Li, Y. W. Lin, B.Q. Sun, D. S. Jiang, and W. K. Ge, Appl. Phys. Lett. **78**, 2217 (2001).

[12] P. Perlin, S. G. Subramanya, D. E. Mars, J. Kruger, N. A. Shapiro, H. Siegle, and E. R. Weber, Appl. Phys. Lett. **73**, 3703 (1998).

[13] W. Shan, W. Walukiewicz, J. W. Ager III, E. E. Haller, J. F. Geisz, D. J. Friedman, J. M. Olson, and S. R. Kurtz, Phys. Rev. Lett. **82**, 1221 (1999).

[14] J. D. Perkins, A. Mascarenhas, J. F. Geisz, and D. J. Friedman, Phys. Rev. B **64**,121301(R) (2001).

[15] W. K. Hung, M. Y. Chern, Y. F. Chen, Z. L. Yang, and Y. S. Huang, Phys. Rev. B **62**, 13028 (2000).

[16] G. Leibiger, V. Gottschalch, B. Rheinländer, J. Sik and M. Schubert, Appl. Phys. Lett. **77**, 1650 (2000).

[17] D. J. Wolford, J. A. Bradley, K. Fry, and J. Thompson, Proc. 17th Conf. of the Physics of Semiconductors (New York: Springer), p. 627 (1984).

[18] X. Liu, M. E. Pistol, L. Samuelson, S. Schwetlick, and W. Seifert, Appl. Phys. Lett. **56**, 1451 (1990).

[19] P. Bhattacharya, *Semiconductor Optoelectronic Devices*, Prentice-Hall (1994).

[20] T. Yang, S. Nakajima and S. Sakai, Japan. J. Appl. Phys. **36**, L320 (1997).

[21] N. Baillargeon, K. Y. Cheng, G. F. Hofler, P. J. Pearah, and K. C. Hsieh, Appl. Phys. Lett. **60**, 2540 (1992).

[22] W. G. Bi and C. W. Tu, Appl. Phys. Lett. **69**, 3710 (1996).

[23] K. M. Yu, W. Walukiewicz, J. Wu, J. W. Beeman, J. W. Ager III, E. E. Haller, W. Shan, H. P. Xin, and C. W. Tu, Appl. Phys. Lett. **78**, 1077 (2001).

[24] J. C. Harmand, G. Ungaro, J. Ramos, E. V. K. Rao, G. Saint-Girons, R. Tessier, G. Le Roux, L. Largeau, and G. Patriarche, J. Cryst. Growth **227-228**, 553 (2001).

[25] B. N. Murdin, N. Kamal-Saadi, A. Lindsay, E. P. O'Reilly, A. R. Adams, G. J. Nott, J. G. Crowder, C. R. Pidgeon, I. V. Bradley, J.-P. R. Wells, T. Burke, A.D. Johnson, and T. Ashley, Appl. Phys. Lett. **78**, 1568 (2001).

[26] R. Bhat, C. Caneau, L. Salamanca-Riba, W. Bi., and C. Tu, J. Cryst. Growth, **195**, 427 (1998).

[27] J. Sik, M. Schubert, G. Leibiger, V. Gottschalch, and G. Wagner, J. Appl. Phys. **89**, 294 (2001).

[28] Y. Zhang, A. Mascarenhas, J. F. Geisz, H. P. Xin, and C. W. Tu, Phys. Rev. B **63**, 085205 (2001).

[29] S.-H. Wei and A. Zunger, Phys. Rev. Lett. **76** , 664 (1996).

[30] U. Tisch, E. Finkman and J. Salzman, Appl. Phys. Lett. **81**, 463 (2002).

[31] Y. Zhang, A. Mascarenhas, H. P. Xin, and C. W. Tu, Phys. Rev. B **61**, 7479 (2000).

[32] T. Mattila, S. H. Wei and A. Zunger, Phys. Rev. B **60**, 11245 (1999).

[33] A. Lindsay and E. P. O'Reilly, Solid State Commun. **112**, 443 (1999).

[34] S. Sakai, Y. Ueta and Y. Terauchi, Japan. J. Appl. Phys. part 1 **32**, 4413 (1993).

[35] E. D. Jones, N. A. Modine, A. A. Allerman, S. R. Kurtz, A. F. Wright, S. T. Tozer, and X. Wei, Phys. Rev. B **60**, 4430 (1999).

[36] W. Shan, W. Walukiewicz, J. W. Ager III, E. E. Haller, J. F. Geisz, D. J. Friedman, J. M. Olson, and S. R. Kurtz, Appl. Phys. Lett. **86**, 2349 (1999).

[37] P. Perlin, P. Wisniewski, C. Skierbiszewski, T. Suski, E. Kaminska, S. G. Subramanya, E. R. Weber, D. E. Mars, and W. Walukiewicz, Appl. Phys. Lett. **76**, 1279 (2000).

[38] J. Hader, S. W. Koch, J. V. Moloney, and E. P. O'Reilly, Appl. Phys. Lett. **76**, 3685 (2000).

[39] C. Skierbiszewski, P. Perlin, P. Wisniewski, T. Suski, J. Geisz, K. Hingerl, W. Janitsch, D. Mars, and W. Walukiewicz, Phys. Rev. B **65**, 35207 (2002).

[40] K. M. Yu, W. Walukiewicz, W. Shan, J. W. Ager III, J. Wu, E. E. Haller, J. F. Geisz, D. J. Friedman, and J. M. Olson, Phys. Rev. B **61**, R13337 (2000).

[41] W. Shan, W. Walukiewicz, K. M. Yu, J. W. Ager III, E. E. Haller, J. F. Geisz, D. J. Friedman, J. M. Olson, S. R. Kurtz, and C. Nauka, Phys. Rev. B **62**, 4211 (2000).

[42] W. Walukiewicz, W. Shan, K. M. Yu, J. W. Ager III, E. E. Haller, I. Mitkowski, M. J. Seong, H. Alawadhi, and A. K. Ramdas, Phys. Rev. Lett. **85**, 1552 (2000).

[43] E. P. O'Reilly and A. Lindsay, Phys. Status Solidi b **216**, 131 (1999).

[44] L. Bellaiche, S-H. Wei and A. Zunger, Phys. Rev. B **56**, 10233 (1997).

[45] L. Bellaiche and A. Zunger, Phys. Rev. B **57**, 4425 (1998).

[46] L. Bellaiche, N. A. Modine and E. D. Jones, Phys. Rev. B **62**, 15311 (2000).

[47] L.-W. Wang, Appl. Phys. Lett. **78**, 1565 (2001).

[48] P. R. C. Kent and A. Zunger, Phys. Rev. Lett. **86**, 2609 (2001).

[49] P. R. C. Kent and A. Zunger, Phys. Rev. B **64**, 115208 (2001).

[50] P. R. C. Kent and A. Zunger, Appl. Phys. Lett. **79**, 2339 (2001).

[51] L. Bellaiche, Appl. Phys. Lett. **75**, 2578 (1999).

[52] T. Kitatani, M. Kondow, T. Kikawa, Y. Yazawa, M. Otai, and K. Uomi, Japan. J. Appl. Phys. Part 1 **38**, 5003 (1999).

[53] B. Q. Sun, D. S. Jiang, X. D. Luo, Z. Y. Xu, Z. Pan, L. H. Li, and R. H. Wu, Appl. Phys. Lett. **76**, 2862 (2000).

[54] P. Krispin, S. G. Spruyette, J. S. Harris, and K. H. Ploog, J. Appl. Phys. **88**, 4153 (2000).

[55] R. H. Ahrenkiel, S. W. Johnston, B. M. Keyes, D. J. Friedman, and S. M. Vernon, Appl. Phys. Lett. **77**, 3794 (2000).

[56] I. A. Buyanova, G. Pozina, P. N. Hai, W. M. Chen, H. P. Xin, and C. W. Tu, Phys. Rev. B **63**, 033303 (2000).

[57] M. Hetterich, M. D. Dawson, A. Yu. Egorov, D. Bernklau, and H. Riechert, Appl. Phys. Lett. **76**, 1030 (2000).

[58] H. P. Xin and C. W. Tu, Appl. Phys. Lett. **72**, 2442 (1998).

[59] T. Miyamoto, K. Takeuchi, T. Kageyama, F. Koyama, and K. Iga, J, Cryst. Growth 197, **67** (1999).

[60] J. S. Harris, IEEE J. Sel. Top. Quantum Electron., 1145 (2000).

[61] S. G. Spruytte, M. C. Larson, W. Wampler, C. Coldren, P. Krispin, H. E. Petersen, S. Picraux, K. Ploog, and J. S. Harris, J. Cryst. Growth **227-228**, 506 (2001).

[62] A. Y. Egorov**,** D. Bernklau, B. Borchert, S. Illek, D. Livshits, A. Rucki, M. Schuster, A. Kaschner, A. Hoffmann**,** Gh. Dumitras, M. C. Amann, and H. Riechert, J. Cryst. Growth **227-8**, 545 (2001).

[63] X. Yang, M. J. Jurkovic, J. B. Heroux, and W. Wang, Appl. Phys. Lett. **75**, 178 (1999).

[64] H. Schimizu, K. Kumada, S. Uchiyama, and A. Kasukawa, Electron. Lett. **36**, 1379 (2000).

[65] X. Yang, J. B. Heroux, L. F. Mei, and W. I. Wang, Appl. Phys. Lett. **78**, 4068 (2001).

[66] W. Ha, V. Gambin, M. Vistey, S. Bank, H. Yuen, S. Kim, and J. S. Harris, IEEE Photonics Technol. Lett. **14**, 591 (2002).

[67] W. Ha, V. Gambin, M. Vistey, S. Bank, H. Yuen, S. Kim, and J. S. Harris, Electron. Lett. **38**, 277 (2002).

[68] G. Steinle, F. Mederer, M. Kircherere, R. Michalzik, G. Kristen, A. Y. Egorov, H. Riechert, H. D. Wolf, and K. Ebeling, Electron. Lett. **37**, 632 (2001).

[69] M. C. Larson, M. Kondow, T. Kitatani, K. Nakahara, K. Tamura, H. Inoue, and K. Uomi, IEEE Photonics Technol. Lett. **10**, 188 (1998).

[70] K. D. Choquette, J. F. Klem, A. I. Fischer, O. Blum, A. A. Allerman, I. J. Fritz, S. R. Kurtz, W. G. Breiland, R. Sieg, K. M. Geib, J. W. Scott, and R. L. Naone, Electron. Lett. **36**, 1388 (2000).

[71] G. Steinle, A.Y. Egorov and H. Riechert, Electron. Lett. **37**, 93 (2001).

[72] S. Sato, N. Nishiyama, T. Miyamoto, T. Takahashi, N. Jikutani, M. Arai, A. Matsutani, F. Koyama, and N. Iga, Electron. Lett. **36**, 2018 (2000).

[73] A. Ramakrishnan, G. Steinle, C. Degen, and G. Ebbinghau, Electron. Lett. **38**, 322 (2002).

[74] D. J. Friedman, J. F. Geisz, S. R. Kurtz, and J. M. Olson, J. Cryst. Growth **195**, 409 (1998).

[75] S. R. Kurtz, A. A. Allerman, E. D. Jones, J. M. Gee, J. J. Banas, and B. E. Hammons, Appl. Phys. Lett. **74**, 729 (1999).

[76] J. F. Geisz, D. J. Friedman, J. M. Olson, S. R. Kurtz, and B. M. Keyes, J. Cryst. Growth **195**, 401 (1998).

[77] S. R. Kurtz, A. A. Allerman, C. H. Seager, R. M. Sieg, and E. D. Jones, Appl. Phys. Lett. **77**, 400 (2000).

[78] W. Li, M. Pessa, J. Toivonen, and H. Lipsanen, Phys. Rev. B **64**, 113308 (2001).

[79] A. Kaschner, T. Luttgert, H. Born, A. Hoffmann, A. Y. Egorov, and H. Riechert, Appl. Phys. Lett. **78**, 1391 (2001).

[80] P. C. Chang, A. G. Baca, N. Y. Li, P. R. Sharps, H. Q. Hou, J. R. Laroche, and F. Ren, Appl. Phys. Lett. **76**, 2788 (2000).

[81] C. Monier, A. G. Baca, P. C. Chang, N. Y. Li, H. Q. Hou, F. Ren, and S. J. Pearton, Electron. Lett. **37**, 198 (2001).

[82] R. J. Welty, H. P. Xin, K. Mochizuki, C. W. Tu, and P. M. Asbeck, Solid-State Electron. **46**, 1 (2002).

[83] H. M. Manasevit and W. I. Simpson, J. Electrochem. Soc. **116**, 1725 (1969).

[84] see, e.g., G. B. Stringfellow, *Organometallic vapor-phase epitaxy: Theory and* practice, Academic Press, San Diego, 1989.

[85] M. E. Heimbuch, A. L. Holmes, Jr., C. M. Reaves, M. P. Mack, S. P. DenBaars, and L. A. Coldren, J. Electron. Mater. **23**, 87 (1994).

[86] F. E.Williams and H. Eyring, J. Chem. Phys. **15**, 289 (1947).

[87] D. J. Keller and F. S. Franke, Surf. Sci. **294**, 409 (1993).

[88] P. F. Fewster, *X-ray Scattering From Semiconductors*, Imperial College Press, London 2000.

[89] A. Authier, *Dynamical Theory of X-ray Diffraction*, Oxford University Press, 2001.

[90] J. C. Harmand, G. Ungaro, L. Largeau, and G. LeRoux, Appl. Phys. Lett. **77**, 2482 (2000).

[91] D. J. Friedman, A. G. Norman, J. F. Geisz, and S. R. Kurtz, J. Cryst. Growth **208**, 11 (2000).

[92] A. J. Ptak, S. Kurtz, C. Curtis, R. Reedy, and J. M. Olson, J. Cryst. Growth **243**, 231 (2002).

[93] S. Kurtz, R. Reedy, G. D. Barber, J. F. Geisz, D. J. Friedman, W. E. McMahon, and J. M. Olson, J. Cryst. Growth **234**, 318 (2002).

[94] N. Q. Thinh, I. A. Buyanova, P. N. Hai, W. M. Chen, H. P. Xin, and C. W. Tu, Phys. Rev. B **63**, 033203 (2001).

[95] N. Q. Thinh, I. A. Buyanova, W. M. Chen, H. P. Xin, and C. W. Tu, Appl. Phys. Lett. **79**, 3089 (2001).

[96] S. G. Spruytte, C. W. Coldren, J. S. Harris, W. Wampler, P. Krispin, K. Ploog, and M. C. Larson, J. Appl. Phys. **89**, 4401 (2001).

[97] T. Ahlgren, E. Vainonen-Ahlgren, J. Likonen, W. Li, and M. Pessa, Appl. Phys. Lett. **80**, 2314 (2002).

[98] W. Li, M. Pessa, T. Ahlgren, and J. Dekker, Appl. Phys. Lett. **79**, 1094 (2001).

[99] E. V. K. Rao, A. Ougazzaden, Y. Le Begallo, and M. Juhel, Appl. Phys. Lett. **72**, 1409 (1998).

[100] L. H. Li, Z. Pan, W. Zhang, Y. W. Lin, Z. Q. Zhou, and R. H. Wu, J. Appl. Phys. **87**, 245 (2000).

[101] Z. Pan, L. H. Li, W. Zhang, Y. W. Lin, and R. H. Wu, Appl. Phys. Lett. **77**, 1280 (2000).

[102] T. Kitatani, K. Nakahara, M. Kondow, K. Uomi, and T. Tanaka, J, Cryst. Growth **209**, 345 (2000).

[103] H. P. Xin, C. W. Tu and M. Geva, Appl. Phys. Lett. **75**, 1416 (1999).

[104] A. Polimeni, H. Baldassari, M. Bissiri, M. Capizzi, M. Fischer, M. Reinhardt, and A. Forchel, Phys. Rev. B **63**, 201304(R) (2001).

[105] H. P. Xin, K. L. Kavanagh and C. W. Tu, J. Cryst. Growth **208**, 145 (2000).

[106] P. J. Klar, H. Grüning, J. Koch, S. Schäfer, K. Volz, W. Stolz, W. Heimbrodt, A. Kamal Saadi, A. Lindsay, and E. P. O'Reilly, Phys. Rev. B **64**, 121203 (2001).

[107] K. Kim and A. Zunger, Phys. Rev. Lett. **86**, 2609 (2001).

[108] S. Kurtz, J. Webb, L. Gedvilas, D. Friedman, J. Geisz, J. Olson, R. King, D. Joslin, and N. Karam, Appl. Phys. Lett. **78**, 748 (2001).

[109] K. Saarinen, P. Hautojärvi and C. Corbel, in *Identification of Defects in Semiconductors*, edited by M. Stavola (Academic, New York, 1998) p. 209.

[110] C.Corbel, F. Pierre, K. Saarinen, P. Hautojärvi, and P. Moser, Phys. Rev. B **45**, 3386 (1992).

[111] R. Rantamäki, T. Tuomi, Z. R. Zytkiewicz, P. J. McNally, and A. N. Danilewsky, J. X-ray Sci. Techn. **8**, 277 (2000).

[112] Y. Shinozuka, Physica B **308-310**, 506 (2001).

[113] D. L. Huffaker, G. Park, Z. Zou, O. B. Shchekin, and D. G. Deppe, Appl. Phys. Lett. **73**, 2564 (1998).

[114] G. Park, O. B. Shchekin, S. Csutak, D. L. Huffaker, and D. G. Deppe, Appl. Phys. Lett. **75**, 3267 (1999).

[115] I. Mukhametzhanov, R. Heitz, J. Zeng, P. Chen, and A. Madhukar, Appl. Phys. Lett. **73**, 1841 (1998).

[116] V. M. Ustinov, N. A. Maleev, A. E. Zhukov, A. R. Kovsh, A. Yu. Egorov, A. V. Lunev, B. V. Volovik, I. L. Krestnikov, Yu. G. Musikhin, N. A. Bert, P. S. Kop'ev, Zh. I. Alferov, N. N. Ledentsov, and D. Bimberg, Appl. Phys. Lett. **74,** 2815 (1999).

[117] K. Nishi, H. Saito, S. Sugou and J-S. Lee, Appl. Phys. Lett. **74**, 1111 (1999).

[118] M. Sopanen, H. P. Xin and C. W. Tu, Appl. Phys. Lett. **76**, 994 (2000).

[119] S. Makino, T. Miyamoto, K. Nageyama, N. Nishiyama, F. Koyama, and K. Iga, J. Cryst. Growth **221**, 561 (2000).

[120] Y. Nakata, K. Mukai, M. Sugawara, K. Ohtsubo, H. Ishikawa, and N.Yokoyama, J. Cryst. Growth **208**, 93 (2000).

[121] H. Saito, K. Nishi and S. Sugou, Appl. Phys. Lett. **74**, 1224 (1999).

[122] J. Oshinowo, M. Nishioka, S. Ishida, and Y. Arakawa, Appl. Phys. Lett. **65**, 1421 (1994).

[123] J. Bloch, J. Shah, W. S. Hobson, J. Lapata, and S. N. G. Chu, Appl. Phys. Lett. **75**, 2199 (1999).

[124] A. Passaseo, G. Maruccio, M. De Vittorio, R. Rinaldi, R. Cingolani, and M. Lomascolo, Appl. Phys. Lett. **78**, 1382 (2001).

[125] N.-T. Yeh, T.-E. Nee, J.-I. Chyi, T. M. Hsu, and C. C. Huang, Appl. Phys. Lett. **76**, 1567 (2000).

[126] M. Sopanen, H. Lipsanen and J. Ahopelto, Appl. Phys. Lett **66**, 2364 (1995).

[127] D. J. Eaglesham and M. Cerullo, Phys. Rev. Lett. **64**, 1943 (1990).

[128] L. Grenouillet, C. Bru-Chevallier, G. Guillot, P. Gilet, P. Duvault, C. Vannuffel, A. Million, and A. Chenevas-Paule, Appl. Phys. Lett. **76**, 2241 (2000).

[129] M.-A. Pinault and E. Tournié , Appl. Phys. Lett. **78**, 1562 (2001).